Dear Editorial Team,

During the review process of the associated paper on the same study we currently have in AMTD (amt-2020-116), we discovered that a correction (increase) of the eddy diffusivity by 25% was required due to a computational error. Due to this correction, all the gradient fluxes presented in this current paper (amt-2020-257) also must be increased by 25%. The IDM fluxes and other results remain unchanged, and the correction does not affect any of the conclusions in this paper.

Because the gradient fluxes changed, figures and tables containing gradient flux results have been changed. Affected tables are Table 2 and Table S1. Affected figures are Figure 2, Figure 4, and Figure 5 in the main text, and Figure S7, S8, S9, S11(a), S13, and S14 in the supplement. The marked-up manuscript is inserted below for your reference.

The 25% increase in gradient fluxes does affect the comparison with the IDM flux; the relative difference changed from 11% to 30%. This change is reflected in the second last sentence of the abstract, the last sentence of Section 3.2, and the middle of the first paragraph in Section 4. This does not change our conclusions.

We have presented results of NH_3 and total alkanes fluxes with gradient and IDM methods in Table 2. In the original manuscript, we showed flux results from IDM method in the abstract, Section 3.6, and Section 4. When revising the manuscript, we thought showing fluxes from the gradient method in those text is more consistent, since we discussed a limitation of NH3 IDM flux in section 3.3. The agreement of total alkane flux with gradient and IDM methods is also discussed, this time at the end of Section 3.4.

Best regards,

Yuan You & Ralf Staebler

Toronto, 18 December 2020

Quantifying fugitive gas emissions from an oil sands tailings pond with open-path FTIR measurements

Yuan You[1,§], Samar G. Moussa[1], Lucas Zhang[2], Long Fu[2], James Beck[3], Ralf M. Staebler[1]

[1] Air Quality Research Division, Environment and Climate Change Canada (ECCC), Toronto, M3H 5T4, Canada
[2]Alberta Environment and Parks, Edmonton, T5J, 5C6, Canada
[3]Suncor Energy Inc., Calgary, T2P 3Y7, Canada
[§]Now at Department of Physics, University of Toronto, Toronto, M5S 1A7, Canada

Correspondence to: Ralf M. Staebler (ralf.staebler@canada.ca)

Abstract. Fugitive emissions from tailings ponds contribute significantly to facility emissions in the Alberta Oil Sands, but details on chemical emission profiles and the temporal and spatial variability of emissions to the atmosphere are sparse, since flux measurement techniques applied for compliance monitoring have their limitations. In this study, open-path Fourier transform infrared spectroscopy was evaluated as a potential alternative method for quantifying spatially representative fluxes for various pollutants (methane, ammonia, and alkanes) from a particular pond, using vertical flux gradient and inverse dispersion methods. Gradient fluxes of methane averaged 4.3 g $m^{-2}d^{-1}$ but were 44% lower than nearby eddy covariance measurements, while inverse dispersion fluxes agreed to within 30%. With gradient fluxes method, significant NH_3 emission fluxes were observed (0.05 g $m^{-2}d^{-1}$ (42 tonnes y^{-1})), and total alkane fluxes were estimated to be 1.05 g $m^{-2}d^{-1}$ (881 tonnes y^{-1}), representing 9.6% of the facility emissions.

Deleted: 3.4
Deleted: 11
Deleted: S
Deleted: 0
Deleted: .
Deleted: 11
Deleted: 92
Deleted: 1.33
Deleted: 1120
Deleted: 12

1 Introduction

Tailings from the oil sands industrial processes in Alberta's Athabasca Oil Sands consist of a mixture of water, sand, non-recovered bitumen, and additives from the bitumen extraction processes (Small et al., 2015). These tailings are deposited into large engineered tailings ponds on site. Separation of processed water from remaining tailings occurs continuously in the tailings pond, and the processed water is recycled (Canada's Oil Sands Tailings Ponds: https://www.canadasoilsands.ca/en/explore-topics/tailings-ponds). The total liquid surface area covered by tailings ponds in the Athabasca Oil Sands was 103 km^2 in 2016 and continues to grow (Alberta Environment and Parks, 2016). Emissions to the atmosphere from tailings ponds include methane (CH_4), carbon dioxide (CO_2), reduced sulfur compounds, volatile organic compounds (VOCs), and polycyclic aromatic hydrocarbons (PAHs) (Siddique et al., 2007; Simpson et al., 2010; Yeh et al., 2010; Siddique et al., 2011; Siddique et al., 2012; Galarneau et al., 2014; Small et al., 2015; Bari and Kindzierski, 2018; Zhang et al., 2019). Emissions from tailings ponds vary with pond conditions, such as pond age and solvents additives in the ponds, and can contribute significantly to total facility emissions (Small et al., 2015).

Deleted: sands

Very few studies focusing on emissions of air pollutants from tailings ponds have been published (Galarneau et al., 2014; Small et al., 2015; Zhang et al., 2019). Compounds of particular interest include alkanes and ammonia (NH_3). Alkanes are part of the solvents used in the extraction process (Small et al., 2015), and can dominate VOCs emissions from oil sands facilities (Li et al., 2017). Previously reported VOCs emissions by facilities had large uncertainties,

especially from fugitive sources, due to limitations of the methods used to estimate emissions for compliance monitoring purposes (Li et al., 2017). VOCs in the atmosphere are important because of their effects on ambient ozone and secondary aerosol formation (Field et al., 2015; Kroll and Seinfeld, 2008). Emissions of NH_3 from tailings ponds to the atmosphere have not been published, although NH_3 has been observed in the oil sands region (Bytnerowicz, et al., 2012; Whaley et al., 2018). NH_3 emissions have important environmental implications, such as forming atmospheric aerosols with sulfuric acid (Kürten, et al., 2016) and affecting nitrogen deposition in the ecosystem (Makar, et al., 2018). This information is important for model simulations of critical loads of acidifying deposition in the ecosystem (Makar, et al., 2018). This field measurement project provided a great opportunity to continuously measure and to quantify tailings pond emissions over more than a month, especially for NH_3 and total alkanes.

Open-path Fourier transform infrared (OP-FTIR) spectroscopy has been considered a good candidate for an alternative method to monitor fugitive emissions from industrial or hazardous waste area sources, since the method is non-intrusive, integrates over long path-lengths, and has the ability to quantify several different gases of interest simultaneously and continuously (Marshall et al., 1994), without sample line issues. It has previously been used to quantify mole fractions of various air pollutants from different sources such as forest fires (Griffith et al., 1991; Yokelson et al., 1996; Yokelson et al., 1997; Goode et al., 1999; Yokelson, 1999; Yokelson et al., 2007; Burling et al., 2010; Johnson et al., 2010; Akagi et al., 2013; Yokelson et al., 2013; Akagi et al., 2014; Paton-Walsh et al., 2014; Smith et al., 2014), volcanoes (Horrocks et al., 1999; Oppenheimer and Kyle, 2008), industrial sites (Wu et al., 1995), harbours (Wiacek et al., 2018), and road vehicles (Bradley et al., 2000; Grutter et al., 2003; You et al., 2017). OP-FTIR measurements with vertically separated paths have previously been conducted to derive emission rate of air pollutants. Schäfer et al. (2012) deployed two OP-FTIR spectrometers with parallel paths 2.2 meter vertically apart at a grassland at Fuhrberg Germany, to measure nitrous oxide (N_2O) emissions with a flux-gradient method, and showed the calculated flux is comparable to the chamber measurements at the same grassland. Flesch et al. (2016) deployed OP-FTIR measurement with one spectrometer and two paths vertically separated by about 1 m on average ("slant path" configuration) at a cattle field in Alberta, Canada. They derived emission rates of N_2O and NH_3 by flux-gradient and inverse-dispersion methods, demonstrating the capability of OP-FTIR systems to measure emission rates of N_2O and NH_3. Following the flux-gradient method in Flesch et al. (2016), Bai et al. (2018) measured the flux of N_2O, NH_3, CH_4, and CO_2 from a vegetable farm in Australia by an OP-FTIR system with two paths vertically separated by 0.5 m on average. At the same vegetable farm, Bai et al. (2019) measured emission rates of N_2O by flux chambers and OP-FTIR "slant path" configuration with flux-gradient methods, and showed a large variation of the ratio of N_2O fluxes with these two measurements. Inverse dispersion models have also been applied to OP-FTIR measurements to quantify emission rates in previous studies (Flesch et al., 2004; Flesch et al., 2005; Bai et al., 2014; Hu et al., 2016; Shonkwiler and Ham, 2018).

Longer continuous coverage with a greater height difference between paths is one distinguishing feature of this study compared to previous research. The motivation of this work is to quantify emission rates of pollutants from one specific tailings pond by combining OP-FTIR measurements with micrometeorological methods. Emissions of CH_4, NH_3, and total alkanes as well as a comparison of gradient and inverse dispersion methods are presented in this study.

2 Open-path FTIR field measurements and methods for deriving fluxes

2.1 Site and measurement set up

The main site of this study was on the south shore of Suncor Pond 2/3 (Fig. 1; 56°59'0.90"N, 111°30'30.30"W, 305m ASL). Sensible heat and momentum fluxes were measured on a mobile tower with sonic anemometers (model CSAT-3, Campbell Scientific, USA) at 8m, 18m, and 32m above ground. Vertical gradients of gaseous pollutant mole fractions were measured by drawing air from 8m, 18m, and 32m on the tower to instrumentation housed in a trailer on the ground. A fourth sample inlet at 4m was on the roof of the main trailer beside the mobile tower. CH_4 and H_2O mole fractions at these 4 levels were measured sequentially by cavity ring-down spectroscopy (CRDS) (model G2204, Picarro, USA). CH_4 mole fractions at 4m were used to calibrate the mole fraction from OP-FTIR retrievals. At 18m, CH_4 mole fractions were also measured by another CRDS (model G2311-f, Picarro, USA) at 10Hz, to be combined with sonic anemometer measurements to calculate the eddy covariance (EC) flux. Meteorological parameters including temperature and relative humidity (RH) were measured at the same three levels on the tower, and 1m above ground. A propeller anemometer (Model 05103-10, Campbell Scientific, USA) on the roof of the main trailer at 4m above ground provided an additional measurement of wind speed and direction. Measurements were conducted from July 28 to September 5, 2017. The FTIR spectrometer was located 10m to the east of the flux tower and the paths were along the south shore of the pond. This manuscript focuses on derived fluxes from the measurement of OP-FTIR. Other experimental details of the project can be found in You et al. (2020).

2.2 Open-path Fourier transform infrared spectrometer (OP-FITR) system

The FTIR measurements were taken with a commercial Open Path FTIR Spectrometer (Open Path Air Monitoring System (OPS), Bruker, Germany), which was setup at 1.7m above the ground in a trailer. The infrared source is an air-cooled Globar. The emitted radiation is directed through the interferometer where it is modulated, travels along the measurement path (200m horizontal distance) to a retroreflector array that reflects the radiation, travels back to the spectrometer, and enters a Stirling-cooled mercury cadmium telluride (MCT) detector (monostatic configuration). Three retroreflectors were employed in this study: one near ground level (1m) on a tripod, and two at higher elevations on basket lifts, resulting in heights of reflectors of approximately 1m, 11m and 23m above ground. Three paths with these three retro-reflectors are referred as bottom, middle and top paths. The bottom retro-reflector was approximately twice the size of the upper two (59 vs. 30 reflector cubes). All retro-reflectors were cleaned with an alcohol solution once during the study, and the bottom mirror were rinsed with de-ionized water three times. Return signal strength decreased by around 65% during the 5-week study due to reflector deterioration, presumably mostly due to impaction by particulate matter. This reflector deterioration also decreased the signal-to-noise by around 67%, based on spectral retrievals for CH_4, but did not affect the mean mole fractions measured.

In this study, spectra were measured at a resolution of 0.5 cm^{-1} with 250 scans co-added to increase signal-to-noise ratio, resulting in roughly a one-minute temporal resolution. Stray light spectra were recorded regularly by pointing the spectrometer away from the retroreflectors. This stray light spectrum accounts for radiation back to the detector

from internal reflections inside the spectrometer, i.e. not from the retroreflector array, and was subtracted from all the measurement spectra before performing further analysis.

Spectral fitting was performed with OPUS_RS (Bruker), which uses a non-linear curve fitting algorithm (You et al., 2017). Spectral windows and interference gases for each gas (Table 1) were determined by optimizing capture of the absorption features while minimizing interferences. To further improve fittings, baselines were optimized through either linear or Gaussian fits under given spectral windows and interfering gases. For CH_4 and CO_2, temperature-dependent reference files were used for fitting and retrieving mole fractions. For other pollutants, reference spectra at 296K were used and retrieved mole fractions were corrected for air density using measured ambient temperature and pressure. For the bottom path, the retrieved mole fractions were corrected for the temperature effect given the temperature difference between the temperatures at 8m (used as the input temperature) and 1m. For the top path, the retrieved mole fractions were corrected for the temperature effect given the temperature difference between the input temperature at 8m and the temperature at12m (linearly estimated by using temperature at 8m and 18m). The corrected mole fractions from the three paths were then converted to dry mole fractions using the RH, temperature and pressure measured at 1m, 8m, and 18m. The dry CH_4 mole fractions from FTIR were then calibrated against CH_4 mole fractions from point cavity ring-down spectrometer (CRDS) measurements (Picarro G2204) at 4 m (Supplemental Material 1.1. Fig. S1). These calibrated CH_4 mole fractions from the FTIR were then used in flux calculations.

We also attempted to retrieve several other pollutants from measured FTIR spectra, but encountered insufficient signal-to-noise ratios, given the existing mole fractions at this location, variability in ambient H_2O vapor, etc. These pollutants include toluene, benzene, xylenes, sulfur dioxide, dimethyl sulfide, carbonyl sulfide, formic acid, and hydrogen cyanide. Given the complex mixture of interfering gas signatures at this site, the detection limits of this open path system were insufficient for flux calculations.

2.3 Method of deriving gradient flux

2.3.1 Method of deriving eddy diffusivity of gas (K_c)

Gradient flux estimates are derived from the vertical gradient of mole fractions and the associated turbulence, given by

$$F_c = -K_c \frac{\partial c}{\partial z} \quad (1)$$

where F_c is the flux for a pollutant gas c, and $\frac{\partial c}{\partial z}$ is the vertical gradient of mole fractions of gas c. K_c is the eddy diffusivity of the gas c, a transfer coefficient characterizing turbulent transport (Monin and Obukhov, 1954) and relating the vertical gradient of gas c to its flux. To calculate the gradient flux of pollutants measured by the OP-FTIR system, K_c has to be calculated first. In this study, K_c is calculated with a variation on the "modified Bowen ratio" method (Meyers et al., 1996; Bolinius et al., 2016), which was described in detail in You et al. (2020). The key steps are repeated here. With the EC flux of CH_4 measured at 18m and mole fraction gradient measured at 8m and 32m by CRDS, K_c was calculated using Eq.(1). The limitation of using this K_c is that when the vertical gradient $\frac{\partial c}{\partial z}$ is close to

zero, both F_c and K_c are poorly defined. A much better behaved eddy diffusivity is that for momentum, calculated by combining the wind profile with the momentum flux (Eq.(2)). To construct a continuous time series of K_c for CH_4, we used K_m and the relationship between K_m and K_c in Eq.(3).

$$F_m = -K_m \frac{\partial u}{\partial z} \tag{2}$$

$$S_c = \frac{K_m}{K_c} \tag{3}$$

K_c can thus be calculated from K_m if the Schmidt Number S_c is known. You et al. (2020) showed the details of two approaches to calculate S_c. In this manuscript, we took the result of stability corrected variable S_c from the second approach in You et al. (2020).

2.3.2 Gradient flux based on OP-FTIR measurements

K_c is a function of height above the surface (Monin and Obukhov, 1954). The K_c calculated above applies to a height of 18m, and needs to be adjusted to the OP-FTIR path heights. In this study, the vertical profiles of the CH_4 mole fractions varied over time and mostly showed linear vertical profiles when the wind was from the pond (Supplemental Material Section 1.2). In the following calculation, the vertical profiles of CH_4 and other gases are considered linear over the entire project. Therefore, the representative average height of the FTIR top path is taken as the height of the middle point (at 12 m). K_{c_FTIR} for gradient flux calculated from the top and bottom FTIR paths has been adjusted linearly based on the $K_{c\_(8m,32m)}$ calculated from point measurements at 8m and 32m on the tower:

Deleted: 2

$$\frac{K_{c\_FTIR}}{K_{c_{(8m,32m)}}} = \frac{\frac{K_{m\_FTIR}}{S_c}}{\frac{K_{m(8m,32m)}}{S_c}} = \frac{K_{m\_FTIR}}{K_{m(8m,32m)}} \tag{4}$$

K_m is a function φ_m, which in turn is a function of stability (z/L), where z is the height above ground and L the Obukhov length:

$$K_m = \frac{k u_* z}{\varphi_m} \tag{5}$$

$$\varphi_m = \begin{cases} 1 + \frac{4.7\,z}{L} & for\ \frac{z}{L} > 0 \quad (stable) \\ 1 & for\ \frac{z}{L} = 0\ (neutral) \\ \left[1 - \frac{15z}{L}\right]^{-1/4} & for\ \frac{z}{L} < 0\ (unstable) \end{cases} \tag{6}$$

Here u_* is the friction velocity. From Equations (4)-(6), $K_{m\_FTIR}/K_{m(8m32m)}$ is calculated for each half-hour period. The FTIR gradient flux is then calculated by multiplying this K_{c_FTIR} by the mole fraction gradient between top and bottom path of the FTIR in Eq (1). The difference between assuming linear and logarithmic vertical profiles of the mole fractions is discussed in the Supplemental Material Section 1.2. The logarithmic vertical profile assumption resulted in average flux which is 19% greater than the average gradient flux calculated with linear vertical profiles.

In addition to calculating gradient fluxes by using CH_4 mole fractions gradient between top and bottom paths, gradient fluxes of CH_4 were also calculated by using mole fractions gradient between middle and bottom paths. Results show that the average gradient fluxes with middle-bottom paths gradient are 29% less than that with top-bottom paths (Supplemental Material Section 1.2, Table S1). These results suggest the gradient fluxes in this study may include uncertainties from the vertical profile of *Kc* which has not been studied much in the past. Lastly, the approach developed by Flesch et al. (2016) was applied and compared to the approach shown above. Fluxes were within 70%. K_c for NH_3 and total alkanes are assumed to be the same as K_c for CH_4.

2.3.3 Inverse dispersion fluxes

Inverse dispersion models (IDMs) are a useful method for deriving emission rates estimates based on line-integrated or point mole fraction measurements downwind of a defined source. IDMs require inputs including the mole fraction measurements, the surface turbulence statistics between the measurements and the source, and the background mole fraction (mole fraction upwind of the source) of the pollutant. In this study, we used WindTrax 2.0 (Thunder Beach Scientific, http://www.thunderbeachscientific.com; Flesch et al., 1995; Flesch et al., 2004), which is based on a backward Lagrangian Stochastic (bLS) model. Details on IDM calculations and resulting CH_4 fluxes were presented in You et al. (2020). Key information is repeated here. The emission rate is derived through:

$$Q = \frac{(C - C_b)}{(\frac{C}{Q})sim} \quad (7)$$

where C is the mole fraction of the pollutant measured at a given location, C_b is the background mole fraction, $(C/Q)_{sim}$ is the simulated ratio (calculated by the bLS model) of the pollutant mole fraction at the site to the emission rate at the specified source. In this study, the inputs of surface turbulence statistics are u_* and L calculated from the ultrasonic anemometer measurements at 8m, ambient temperature measured at 8m, and the mean wind direction measured by the propeller anemometer at 4m. All surface turbulence statistics inputs were half-hour averages. Half-hour periods when u_*<0.15 ms^{-1} were excluded (Flesch et al., 2004). IDM fluxes of NH_3 and total alkane are shown in this work for the first time for comparison with gradient fluxes. Meteorological inputs for calculating inverse dispersion fluxes of NH_3 and total alkanes are the same as for CH_4 fluxes. CH_4, NH_3, and total alkanes mole fraction inputs were mole fractions from the bottom path of OP-FTIR.

3 Results and discussion

3.1 Meteorological conditions

The measurement site including the OP-FTIR was at the south shore of the pond (Fig. 1), therefore the north wind (wind direction (WD) ≥ 286° or WD ≤ 76°) was defined as the wind coming from the pond (You et al., 2020). The wind came from the north for about 22% of the entire measurement period (You et al. (2020), Fig. S2). There was no significant diurnal variation in wind direction during the study period. Detailed ambient temperature, water surface temperature, wind speed, and other meteorological parameters can be found in You et al. (2020). As discussed in You

Deleted: S1

et al. (2020), the warm pond surface resulted in continuing convective turbulence at night, resulting in continuing transport of pollutants from the pond into the atmosphere without significant diurnal variation.

Gradient and IDM fluxes for NH_3 and total alkanes are averages for half hour periods when the wind came from the pond. The half-hour fluxes were binned into 16 wind direction sectors, and the area-weighted averages of fluxes from the pond were calculated as described in You et al. (2020).

3.2 Methane

Path-integrated mole fractions and associated gradient fluxes of CH_4 from OP-FTIR are presented here to test if the gradient fluxes derived from the mole fractions with OP-FTIR are comparable to CH_4 fluxes from EC and IDM methods (You et al. (2020)). The area-weighted flux statistics from different methods are summarized in Table 2. The path-integrated measurement from the FTIR bottom path clearly indicates that the CH_4 mole fraction was elevated when the wind was from the pond direction, while it was steady near 2 ppm when the wind was from other directions (Fig. S2 and S3). In addition, a clear vertical gradient (Fig. S3), with mole fractions along the bottom path on the order of 0.5 ppm to 1ppm higher than mole fractions from the top path, identified the pond as the CH_4 source. The fact that the CH_4 mole fraction increased when the wind was from the pond direction, and decreased with height, clearly points to the pond as the dominant local source.

For comparison, vertical profiles of the CH_4 mole fraction by point measurements on the nearby tower are given in Supplemental Material Section 1.2. A linear vertical extrapolation of the profiles to the point where the mole fraction reaches 2.0 ppm (background levels) indicated a median plume height of 64m (Fig. S4 and Fig. S5).

The gradient flux derived from the OP-FTIR shows that the flux was minimal when the wind was from other directions, except for the sector centered at 270° (Fig. 2), which represented a mix of pond and shoreline influences). The average and interquartile ranges of fluxes in wind direction sectors centered at 315°, 337.5° and 0° are comparable. This gradient flux result is consistent with the EC fluxes measured on the adjacent flux tower (You et al. 2020), and these results also suggest that the pond is the main source of measured CH_4 fluxes. However, the sector centered at 292.5° shows average flux 22% and 73% greater than sectors centered at 315° and 337.5°. This is different from the EC fluxes which showed closer agreement between the 292.5°, 315°, 337.5° and 0° sectors (You et al., 2020, Fig. 7). The footprint of the EC fluxes measured on the adjacent flux tower at 18m was calculated by using the Flux Footprint Prediction (FFP) model in Kljun et al. (2015), and results showed the 80% contribution distance was typically within 1km which is closer to the main site than the north edge of pond liquid surface (Fig. 1; You et al. (2020)). The outfall was about 1.4 km from the main site. The discrepancy suggests that the footprint of the gradient method incorporated emissions from the outfall more clearly than the smaller footprint of the EC method.

FTIR CH_4 gradient fluxes and EC fluxes showed a linear correlation, but on average, the gradient fluxes were lower than the EC fluxes by 44% (r^2=0.63) (Fig. S7). In agreement with EC, the gradient flux showed no significant diurnal variations when the wind was from the pond (Fig. S8, with a relative standard deviation of 38%). To investigate the difference between CH_4 gradient fluxes derived from FTIR and EC fluxes, the latter were examined in relation to meteorological conditions, similar to the analysis presented in You et al. (2020). The analysis in You et al. (2020) showed weak correlation between EC flux and friction velocity (u_*) or wind speed, consistent with the observation of

Deleted: eddy covariance

Deleted: 2

Deleted: eddy covariance

Deleted: eddy covariance

Deleted: eddy covariance

Deleted: eddy covariance (

Deleted:)

Deleted: no

Deleted: while

the weak correlation between gradient flux and wind speed (You et al. (2020) Fig. S5). As described in Supplemental Material Section 1.2 (Fig. S4, S5, and S6), CH_4 vertical profiles were closer to linear when the wind speed was less than 6 m/s, and were more logarithmic with wind speed greater than 6 m/s. The sector centered at 292.5° was often associated with wind speeds greater than 6 m/s (21% of the time). The approximation of linear vertical profile could have underestimated the CH_4 flux with periods of high winds by 19%. This weak dependence of gradient flux on wind speed may reflect the uncertainty in the vertical profile of K_c in the calculation of gradient flux.

Model calculations by Horst (1999) showed that the estimated footprint of a gradient flux measurement at the geometric mean height of the gradient is similar to the footprint of EC flux at that same height, for homogeneous upwind area sources. However, mole fraction footprints are significantly larger than perturbation (flux) footprints (Schmid, 1994), and some CH_4 sources on the far shore (e.g. the outfall) may have contributed to the upper path CH_4 mole fraction. This decreased the vertical gradient difference and thus the derived flux relative to the EC flux with its smaller footprint, since the latter is more likely to represent water surface emissions only. As an approximate estimation, the footprint of the path-integrated mole fraction of the top path is about 2.3 km (23m × 100, Flesch et al. (2016)), and this covers the whole pond including the north edge (Fig. 1).

Background mole fractions, upwind of the source under investigation, must be provided for the bLS calculations of CH_4 fluxes. We quantified these using two methods. First, the background mole fraction was determined with the FTIR measurements at the south of the pond, as follows: for most of the days, it was taken as the minimum CH_4 mole fraction from the FTIR bottom path on each day while the wind direction was between 180° and 240°. On Aug 7th and 30th, there was no half-hour period when the wind was from this sector, and the background mole fraction was chosen as the minimum mole fraction for the day. For Aug 1st, there was also no half-hour period for this sector, and the minimum of the day was 2.40 ppm, significantly greater than the minimum mole fraction of other days. Therefore, the background mole fraction of the previous day, 1.92 ppm was used for Aug 1st.

Alberta Environment and Parks (AEP) conducted OP- FTIR measurements (RAM2000 G2; KASSAY FSI, ITT Corp., Mohrsville, PA, USA) at the north side of the pond (Fig. 1), quantifying CH_4 to be used as the second estimate of background mole fractions. For most of the days, the half-hour averaged mole fractions were directly used as the background mole fractions. From Aug 3rd 22:00 to Aug 4th 13:30, Aug 6th 08:00 to 17:00, Aug 23rd 1:30 to 2:00, there were no data from AEP, so background mole fractions for these periods were picked as the interpolation of mole fractions before and after this period. In this approach, the bLS flux results can be negative when the AEP mole fraction is greater than the mole fraction from the measurements at the south shore, possibly due to influences by other emission sources in the surrounding area, gas diffusion under low wind speeds, plume inertia when wind directions changes suddenly, or instrument mismatch differences.

CH_4 IDM fluxes with background determined from the first approach (using measurements at the south of the pond) agreed with IDM fluxes with background determined from the second approach (using measurements at the north of the pond), with a linear regression r^2 of 0.92, and a slope of 0.90; there was a 20% difference between average fluxes from the two approaches (Fig. S10; Table S1). These results confirm that the CH_4 flux estimate from this inverse dispersion approach is consistent and that the first approach to determining backgrounds is appropriate. In the following results and discussion, IDM fluxes with background mole fractions from the first method are used.

Deleted: is observed

Deleted: S9

Formatted: Not Highlight

Deleted: eddy covariance

IDM and EC flux showed moderate comparison (slope=0.69, r=0.62, You et al., (2020), Fig.S7), although the mean IDM fluxes are 30% smaller than EC flux.

3.3 NH_3

The mole fraction of NH_3 was elevated when the wind was from the pond, but was mainly below 5 ppb when the wind was from the south (Fig. 3(a)). NH_3 gradient fluxes were significant when the wind came from the pond direction (Fig. 4(a)).

The time series of mole fraction vertical gradient of NH_3 and CH_4 were similar (Fig. S3). The NH_3 gradient flux and CH_4 gradient flux showed good correlation (r^2=0.7, Fig. 5(a)). The diurnal variation in NH_3 gradient flux (relative standard deviation =72%) was stronger than for the CH_4 gradient flux (relative standard deviation =36%), with greater fluxes from 13:00 to 18:00 MDT (Mountain Daylight savings Time) (Fig. S11(a)). Previous studies showed tailings pond waters contained elevated NH_3 concentrations, which makes them potential sources of NH_3 to the atmosphere (Allen, 2008; Risacher et al., 2018). NH_3 in the pond is mainly produced through nitrate and/or nitrite reduction during microbial activities (Barton and Fauque, 2009; Collins et al., 2016). In addition, some of these nitrate and/or nitrite reduction microbes may also produce reduced sulfur (Barton and Fauque, 2009). The water sample collected from Pond2/3 on August 2017 during this study was alkaline (pH = 8.0 ± 0.5), which also supports the emission of NH_3.

The average flux in the sector centered at 292.5° was 33% and 57% more than the average flux in the sectors centered at 315° and 337.5°, but the median fluxes in these three sectors are within 14%. These suggest the high average flux in 281-304° is skewed by big spikes which are associated with the outfall (with wind directions in 281-304°), but the majority of NH_3 fluxes in the 281-304° wind sector correlated well with CH_4 fluxes which were less affected by the outfall. Although hydrotreating processes in upgraders remove most of the sulfur and nitrogen from the bitumen residue, a small amount of NH_3 might still be carried with the processed water and tailings (Bytnerowicz et al., 2010), and transported with the outfall liquid into the pond. The negative fluxes observed for the 67.5° sector may be due to elevated NH_3 plumes originating from the upgrader facility 3 km upwind in this direction, resulting in a negative gradient and thus deposition to the pond under some circumstances.

IDM fluxes of NH_3 were calculated the same way as CH_4, and show a weak correlation with CH_4 IDM fluxes (Fig. 5(b)). The NH_3 background mole fraction was based on the mean daily minimum, approximately 1ppb (Fig. 3). Vertical profiles of NH_3 mole fraction (Fig. S12) with northerly wind also show roughly linear profiles similar to CH_4. Profiles of sectors centered at 292.5° and 315° are linear. Therefore, the outfall on average did not significantly contribute to the NH_3 profile, i.e. the pond surface was the main source of NH_3. NH_3 fluxes from the gradient method were significantly less than from the IDM method. This difference is mostly due to the input background NH_3 mole fraction. The background NH_3 mole fraction was not measured, and could be greater than 1 ppb if there was any source to the north of the pond. Assuming the NH_3 gradient flux as a reference, different backgrounds were tested in IDM to match the mean gradient flux. A background of 7 ppb of NH_3 was required to close the gap between gradient and IDM fluxes. This seems large but cannot be verified, since there was no ground level measurement of NH_3 near the north of the pond. This illustrates the advantage of using either EC or gradient flux measurements, which are based on mole

Deleted: good
Deleted: 0.93
Deleted: 2
Deleted: 0.46
Deleted: 8(b)
Deleted: .
Deleted: The interquartile range of the fluxes from these two methods overlap, and
Deleted: 11
Deleted: eddy covariance

fraction fluctuations or gradients at a single location and are therefore independent of upwind background mole fraction.

3.4 Total alkane

Total alkane derived from FTIR spectra used butane and octane as two surrogates in this study, following the method in EPA OTM10 (Thoma et al., 2010). Results only reflect alkanes which have similar absorption features as butane and octane, and cannot accurately represent other VOCs. Total alkane fluxes from the pond were evident (Fig. 4(b)). A comparison to CH_4 fluxes showed only a weak correlation (r^2=0.3, Fig. S13), unlike the correlation between NH_3 and CH_4 (Fig. 5(a)). This difference can be explained by sources of alkane and CH_4 at this site. Figure 4(b) shows the average flux from the sector centered at 292.5° is 2.4 g m^{-2} d^{-1}, which is 2.09 and 2.29 times of the average fluxes from the sectors centered at 315° and 337.5°. Figure 2 shows that the average fluxes of CH_4 from the sector centered at 292.5° is 1.22 and 1.72 times of the average fluxes from sectors centered at 315° and 337.5°. These results indicate that there was an enhanced contribution (27%) from around 281° to 304° to total alkane flux measured at the site, but not to the observed CH_4 flux. This enhancement of alkane flux is likely due to the outfall, which was at the edge of the pond, 1.9 km from the site at 295°. The liquid mixture flowing into the pond contained naphthenic solvent which include a mixture of alkanes, alkenes, and aromatic hydrocarbons, and since the outfall is at a temperature of approximately 33°C, enhanced evaporation of volatile components can be expected from this area. The outfall also introduces some mechanical mixing in the upper layers of the pond water, which may contribute to elevated emission rates. The diurnal variation of total alkane gradient flux when the wind came from the pond direction was also weak (the standard deviation of average fluxes at each hour is comparable to the interquartile ranges, Fig. S14). The vertical profiles of total alkane mole fraction with northeastern winds were vertically invariant (Fig. S15). With northwestern winds, profiles showed a decrease mole fraction from bottom to middle path and minimal decrease or even increase from middle to the top path. These total alkane vertical profiles with northern wind, which are different from CH_4 or NH_3 profiles, suggesting there were additional sources other than the pond surface to measured total alkane flux, such as the outfall, and industrial activities upwind. IDM flux of total alkanes agreed moderately with gradient flux, with difference of 21% (26%) in the pond average (median) flux.

Deleted: 1.9

3.5 Methanol (CH_3OH)

Unlike pollutants studied above, the CH_3OH mole fraction did not show significant enhancement when wind was from the pond (Fig. S16), suggesting the pond was not significantly contributing to CH_3OH compared to potential sources surrounding the pond. Gradient flux of CH_3OH was attempted to calculate in the same way as for the other pollutants, and the flux was on the order of 1 mg $m^{-2}day^{-1}$, but with an uncertainty that made it not statistically different from zero. The lifetime of CH_3OH is around 10 days (Simpson et al., 2011; Shephard et al., 2015), and the main source is vegetation (Millet et al., 2008). The mole fractions observed at the site were consistent with satellite measurements representative of the general oil sand region (Shephard et al., 2015), and with an airborne study of VOCs (Simpson et al., 2010). In addition to emissions from vegetation, CH_3OH observed in the oil sands region could

be due to transport from biomass burning (Simpson et al., 2011; Bari and Kindzierski, 2018), and local traffic (Rogers et al., 2006; You et al., 2017).

3.6 Comparison of calculated fluxes to reported emissions and approaches

As a test of the robustness of these results, fluxes of CH_4, NH_3 and total alkane are also calculated from the "slant path" method described by Flesch et al. (2016). Calculation inputs and results are summarized in the Supplemental Material Section 5. Compared to results from our flux gradient approach, CH_4, NH_3, and total alkane fluxes with the "slant path" flux-gradient method were reasonably comparable (24%, 25%, and 30% lower, respectively (Table S1)). The difference in fluxes from the two approaches could be due to differences in assumptions regarding the vertical profiles. In our gradient flux approach, we used linear vertical mole fraction profiles of pollutants to calculate the difference of mean heights between the two paths. In Flesch et al. (2016) the gradient flux for pairs of points along the two paths was integrated along the entire path length assuming the flux was uniform horizontally. In that approach, the dependence of K_c on height is incorporated explicitly, assuming a logarithmic wind profile including a stability correction. In our gradient flux approach, K_c is derived from a measured and stability corrected K_m, and therefore did not require a wind profile shape assumption.

To facilitate a transparent comparison of the emission results from this study to reported facility wide emissions of Suncor, we present emission rates based on simple extrapolation of the measured August emissions to the whole year. Other possible seasonal emission profiles have been reported (Small et al., 2015); using these to convert from August emissions to annual average values would for example result in a scale factor of 0.92 (mass transfer model), 0.64 (mass transfer model adjusted for ice cover), or 0.42 (thawing degree-day model) (Cumulative Environmental Management Association, 2011). The seasonally invariant total emission estimate for NH_3 and total alkanes from Pond 2/3 to the air were 42 and 881 tonnes y^{-1} in 2017, converted from gradient fluxes results in g m^{-2} day^{-1}. However, NH_3 emissions from Pond 2/3 have not been reported in the past, because NH_3 was not being measured as part of compliance flux chamber monitoring. Therefore, the facility wide NH_3 emissions reported to the Government of Canada National Pollutant Release Inventory (NPRI) (0.82 tonnes y^{-1}) in 2017 did not include fugitive emissions from tailings ponds. The solvents entering this tailings pond are naphtha additives with octane, nonane and heptane as the biggest contributors. Li et al. (2017) quantified alkane emissions (including n-alkanes, branched-alkanes, and cycloalkanes) as 36.2 tonnes d^{-1} from the whole facility using airborne measurements in 2013, which is 73.9% of 49 tonnes d^{-1} total VOC emission. Alkanes account for 54% of total VOC emitted from Pond_2/3 in 2017 (internal communication with Samar Moussa). If we use reported facility wide VOC annual emissions in 2017 (17242 tonnes y^{-1}, NPRI) to estimate facility wide total alkane annual emission, we obtain 17242 × 53% = 9138 tonnes y^{-1}, and total alkane emissions from Pond_2/3 contribute 9.6 % to facility wide emissions for 2017. The fugitive NH_3 emissions from Pond_2/3 in this study were 42 tonnes y^{-1}, a number that is 113 times the process related emission number reported for the facility to NPRI. Negligible volume of ammonia may be carried over to the pond through the naphtha recovery unit and FTT line and it is believed that the ammonia is mainly generated from the biogenic activities in the MFT layer of the pond. The majority of H_2S, NH_3 and CH_4 emissions are related to microbiological activities as evidenced in this study.

Deleted: 92

Deleted: 1120

Deleted: 12

Deleted: 92

4 Conclusions and Implications

We have shown that OP-FTIR is an effective method to quantify mole fractions and vertical gradients of CH_4, NH_3, and total alkanes continuously and simultaneously for an area source such as a tailings pond. Benefits are the integration of mole fractions over long path lengths, thus providing a spatially representative average, and the avoidance of sample line issues that can be serious problems for sticky gases such as NH_3. Results from the gradient flux method and IDM calculations suggest OP-FTIR is a useful tool for deriving emission rates of CH_4, NH_3 and total alkane from this type of fugitive area source. For the two approaches of determining background mole fractions of CH_4 with the IDM method, i.e., upwind background measurement vs. local background estimation, the area weight-averaged fluxes of CH_4 were within 20%. FTIR CH_4 gradient fluxes and EC fluxes showed a linear correlation, but on average, the gradient fluxes were lower than the EC fluxes by 44%. CH_4 IDM and EC flux showed moderate comparison, and the mean IDM fluxes are 30% smaller than the EC mean flux. NH_3 gradient flux and IDM flux showed a difference of more than 50%, which suggests that there may have been sources of NH_3 upwind (north) of the pond that were not captured by assuming that southern and northern background NH_3 were similar, thus illustrating a limitation of the IDM method. CH_4, NH_3, and total alkane fluxes were also calculated using the "slant path" flux-gradient method (Flesch et al. 2016), to compare to the our flux gradient approach, and results from the slant path method were reasonably comparable (24%, 25%, and 30% lower, respectively).

The NH_3 emissions results in this study are the first to quantify NH_3 fugitive fluxes from a tailings pond and clearly showed that Pond2/3 is a significant source of NH_3, most likely through microbial activities in the pond. This suggests that at least some tailings ponds in the oil sands could be significant sources of NH_3, compared to process-related facility emissions. Further measurements of NH_3 emissions from tailings ponds are recommended to elucidate our understanding of the mechanisms behind NH_3 emissions and to improve the total facility emission estimates reported to NPRI.

Total alkane gradient fluxes from OP-FTIR measurements clearly showed that the pond is a significant source of total alkane, and annual alkane emissions extrapolated from gradient flux method represented 9.6% of facility emissions. The outfall area contributed significantly (27%) to pond alkane emissions, showing spatial variability of alkane emissions from the pond. Observed CH_3OH mole fractions show that the pond was unlikely a significant source of CH_3OH. This study demonstrated the applicability of OP-FTIR combined with gradient flux or inverse dispersion methods for determining emission fluxes of multiple gases simultaneously, with high temporal resolution and comprehensive spatial coverage.

Deleted: good

Deleted: 11

Deleted: A

Deleted: these measurements

Deleted: 12

Data availability.

All data are publicly available at http://data.ec.gc.ca/data/air/monitor/source-emissions-monitoring-oil-sands-region/emissions-from-tailings-ponds-to-the-atmosphere-oil-sands-region/.

Author contributions.

YY and RS wrote the manuscript; SM, LZ, LF and JB contributed data and comments.

Competing interests.

Dr. Beck is an employee of Suncor Energy. The other authors have no competing interests.

Acknowledgements.

The authors thank the technical team of Andrew Sheppard, Roman Tiuliugenev, Raymon Atienza and Raj Santhaneswaran for their invaluable contributions throughout, Julie Narayan for spatial analysis, Stewart Cober for management and Stoyka Netcheva for home base logistical support. We thank Suncor and its project team (Dan Burt et al.), AECOM (April Kliachik, Peter Tkalec) and SGS (Nathan Grey, Ardan Ross) for site logistics support. This work was partially funded under the Oil Sands Monitoring Program and is a contribution to the program but does not necessarily reflect the position of the program. We also acknowledge funding from the Program for Energy Research and Development (Natural Resources Canada) and from the Climate Change and Air Pollution Program (ECCC).

References

Alberta Environment and Parks, Total Area of the Oil Sands Tailings Ponds over Time: http://osip.alberta.ca/library/Dataset/Details/542, 2016. Last accessed: Sept 22, 2019.

Canada's Oil sands. Tailings Ponds: https://www.canadasoilsands.ca/en/explore-topics/tailings-ponds, Last accessed: Sept 29th, 2019.

Akagi, S. K., Yokelson, R. J., Burling, I. R., Meinardi, S., Simpson, I., Blake, D. R., McMeeking, G. R., Sullivan, A., Lee, T., Kreidenweis, S., Urbanski, S., Reardon, J., Griffith, D. W. T., Johnson, T. J., and Weise, D. R.: Measurements of reactive trace gases and variable O_3 formation rates in some South Carolina biomass burning plumes, Atmos. Chem. Phys., 13, 1141-1165, http://doi.org/10.5194/acp-13-1141-2013, 2013.

Akagi, S. K., Burling, I. R., Mendoza, A., Johnson, T. J., Cameron, M., Griffith, D. W. T., Paton-Walsh, C., Weise, D. R., Reardon, J., and Yokelson, R. J.: Field measurements of trace gases emitted by prescribed fires in southeastern US pine forests using an open-path FTIR system, Atmos. Chem. Phys., 14, 199-215, http://doi.org/10.5194/acp-14-199-2014, 2014.

Allen, E. W.: Process water treatment in Canada's oil sands industry: I. Target pollutants and treatment objectives, J. Environ. Eng. Sci., 7, 123-138, http://doi.org/10.1139/S07-038, 2008.

Bai, M., Suter, H., Lam, S. K., Sun, J., and Chen, D.: Use of open-path FTIR and inverse dispersion technique to quantify gaseous nitrogen loss from an intensive vegetable production site, Atmos. Environ., 94, 687-691, http://doi.org/10.1016/j.atmosenv.2014.06.013, 2014.

Bai, M., Suter, H., Lam, S. K., Davies, R., Flesch, T. K., and Chen, D.: Gaseous emissions from an intensive vegetable farm measured with slant-path FTIR technique, Agric. For. Meterol., 258, 50-55, http://doi.org/10.1016/j.agrformet.2018.03.001, 2018.

Bai, M., Suter, H., Lam, S. K., Flesch, T. K., and Chen, D.: Comparison of slant open-path flux gradient and static closed chamber techniques to measure soil N_2O emissions, Atmos. Meas. Tech., 12, 1095-1102, http://doi.org/10.5194/amt-12-1095-2019, 2019.

Bari, M. A., and Kindzierski, W. B.: Ambient volatile organic compounds (VOCs) in communities of the Athabasca oil sands region: Sources and screening health risk assessment, Environ. Pollut., 235, 602-614, http://doi.org/10.1016/j.envpol.2017.12.065, 2018.

Bolinius, D. J., Jahnke, A., and MacLeod, M.: Comparison of eddy covariance and modified Bowen ratio methods for measuring gas fluxes and implications for measuring fluxes of persistent organic pollutants, Atmos. Chem. Phys., 16, 5315-5322, http://doi.org/10.5194/acp-16-5315-2016, 2016.

Bradley, K. S., Brooks, K. B., Hubbard, L. K., Popp, P. J., and Stedman, D. H.: Motor vehicle fleet emissions by OP-FTIR, Environ. Sci. Tech., 34, 897-899, http://doi.org/10.1021/es9909226, 2000.

Burling, I. R., Yokelson, R. J., Griffith, D. W. T., Johnson, T. J., Veres, P., Roberts, J. M., Warneke, C., Urbanski, S. P., Reardon, J., Weise, D. R., Hao, W. M., and De Gouw, J.: Laboratory measurements of trace gas emissions from biomass burning of fuel types from the southeastern and southwestern United States, Atmos. Chem. Phys., 10, 11115-11130, http://doi.org/10.5194/acp-10-11115-2010, 2010.

Bytnerowicz, A., Fraczek, W., Schilling, S., and Alexander, D.: Spatial and temporal distribution of ambient nitric acid and ammonia in the Athabasca Oil Sands Region, Alberta, J. Limnol., 69, 11-21, 10.3274/JL10-69-S1-03, 2010.

Collins, C. E. V., Foght, J. M., and Siddique, T.: Co-occurrence of methanogenesis and N_2 fixation in oil sands tailings, Sci. Total Environ., 565, 306-312, https://doi.org/10.1016/j.scitotenv.2016.04.154, 2016.

Cumulative Environmental Management Association: Protocol for Updating and Preparing a Modelling Emission Inventory, http://library.cemaonline.ca/ckan/dataset/4cbfe171-aab8-49f8-8d67-118e6840d974/resource/8f449c5d-3129-4d6f-a530-46ec33a46208/download/protocolforupdatingandpreparingamodelling.pdf, 2011. Last accessed Feb 26, 2020.

Field, R.A., Soltis, J., McCarthy, M. C., Murphy, S., and Montague, D. C.: Influence of oil and gas field operations on spatial and temporal distributions of atmospheric non-methane hydrocarbons and their effects on ozone formation in winter, Atmos. Chem. Phys., 15, 3527-3542, https://doi.org/10.5194/acp-15-3527-2015, 2015.

Flesch, T., Wilson, J., Harper, L., and Crenna, B.: Estimating gas emissions from a farm with an inverse-dispersion technique, Atmos. Environ., 39, 4863-4874, http://doi.org/10.1016/j.atmosenv.2005.04.032, 2005.

Flesch, T. K., Wilson, J. D., and Yee, E.: Backward-time Lagrangian stochastic dispersion models and their application to estimate gaseous emissions, J. Appl. Meteorol., 34, 1320-1332, https://doi.org/10.1175/1520-0450(1995)034<1320:BTLSDM>2.0.CO;2, 1995.

Flesch, T. K., Wilson, J. D., Harper, L. A., Crenna, B. P., and Sharpe, R. R.: Deducing ground-to-air emissions from observed trace gas concentrations: A field trial, J. Appl. Meteorol., 43, 487-502, https://doi.org/10.1175/1520-0450(2004)043<0487:DGEFOT>2.0.CO;2, 2004.

Flesch, T. K., Baron, V. S., Wilson, J. D., Griffith, D. W. T., Basarab, J. A., and Carlson, P. J.: Agricultural gas emissions during the spring thaw: Applying a new measurement technique, Agric. For. Meterol., 221, 111-121, https://doi.org/10.1016/j.agrformet.2016.02.010, 2016.

Foght, J. M., Gieg, L. M., and Siddique, T.: The microbiology of oil sands tailings: Past, present, future, FEMS Microbiol. Ecol., 93, https://doi.org/10.1093/femsec/fix034, 2017.

Galarneau, E., Hollebone, B. P., Yang, Z., and Schuster, J.: Preliminary measurement-based estimates of PAH emissions from oil sands tailings ponds, Atmos. Environ., 97, 332-335, https://doi.org/10.1016/j.atmosenv.2014.08.038, 2014.

Goode, J. G., Yokelson, R. J., Susott, R. A., and Ward, D. E.: Trace gas emissions from laboratory biomass fires measured by open-path Fourier transform infrared spectroscopy: Fires in grass and surface fuels, J. Geophys. Res., 104, 21237-21245, https://doi.org/10.1029/1999JD900360, 1999.

Government of Canada, National Pollutant Release Inventory: https://pollution-waste.canada.ca/national-release-inventory/archives/index.cfm?do=facility_substance_summary&lang=en&opt_npri_id=0000002230&opt_report_year=2017. Last access: Jan 07, 2020.

Griffith, D. W. T., Mankin, W. G., Coffey, M. T., Ward, D. E., and RieBau, A.: "FTIR remote sensing of biomass burning emissions of CO_2, CO, CH_4, CH_2O, NO, NO_2, NH_3, and N_2O." Global biomass burning: atmospheric, alimate, and biospheric implications. MIT Press., Cambridge, MA, 1991.

Grutter, M., Flores, E., Basaldud, R., and Ruiz-Suarez, L. G.: Open-path FTIR spectroscopic studies of the trace gases over Mexico City, Atmos. Oceanic Opt., 16, 232-236, 2003.

Horrocks, L., Burton, M., Francis, P., and Oppenheimer, C.: Stable gas plume composition measured by OP-FTIR spectroscopy at Masaya Volcano, Nicaragua, 1998-1999, Geophys. Res. Lett,, 26, 3497-3500, https://doi.org/10.1029/1999GL008383, 1999.

Horst, T. W.: The footprint for estimation of atmosphere-surface exchange fluxes by profile techniques, Boundary Layer Meteorol., 90, 171-188, https://doi.org/10.1023/A:1001774726067, 1999.

Hu, N., Flesch, T. K., Wilson, J. D., Baron, V. S., and Basarab, J. A.: Refining an inverse dispersion method to quantify gas sources on rolling terrain, Agric. For. Meterol., 225, 1-7, https://doi.org/10.1016/j.agrformet.2016.05.007, 2016.

Johnson, T. J., Profeta, L. T. M., Sams, R. L., Griffith, D. W. T., and Yokelson, R. L.: An infrared spectral database for detection of gases emitted by biomass burning, Vib. Spectrosc., 53, 97-102, https://doi.org/10.1016/j.vibspec.2010.02.010, 2010.

Kljun, N., Calanca, P., Rotach, M. W., and Schmid, H. P.: A simple two-dimensional parameterisation for Flux Footprint Prediction (FFP), Geosci. Model Dev., 8, 3695-3713, https://doi.org/10.5194/gmd-8-3695-2015, 2015.

Kroll, J, and Seinfeld, J. H.: Chemistry of secondary organic aerosol: Formation and evolution of low-volatility organics in the atmosphere, Atmos. Environ., 3593-3624, https://doi.org/10.1016/j.atmosenv.2008.01.003, 2008.

Kürten, A., Bianchi, F., Almeida, J., Kupiainen-Määttä, O., Dunne, E. M., Duplissy, J., Williamson, C., Barmet, P., Breitenlechner, M., Dommen, J., Donahue, N. M., Flagan, R. C., Franchin, A., Gordon, H., Hakala, J., Hansel, A., Heinritzi, M., Ickes, L., Jokinen, T., Kangasluoma, J., Kim, J., Kirkby, J., Kupc, A., Lehtipalo, K., Leiminger, M., Makhmutov, V., Onnela, A., Ortega, I. K., Petäjä, T., Praplan, A. P., Riccobono, F., Rissanen, M. P., Rondo, L., Schnitzhofer, R., Schobesberger, S., Smith, J. N., Steiner, G., Stozhkov, Y., Tomé, A., Tröstl, J., Tsagkogeorgas, G., Wagner, P. E., Wimmer, D., Ye, P., Baltensperger, U., Carslaw, K., Kulmala, M., and Curtius, J.: Experimental

particle formation rates spanning tropospheric sulfuric acid and ammonia abundances, ion production rates, and temperatures, J. Geophys. Res., 121, 12,377-312,400, https://doi.org/10.1002/2015JD023908, 2016.

Li, S. M., Leithead, A., Moussa, S. G., Liggio, J., Moran, M. D., Wang, D., Hayden, K., Darlington, A., Gordon, M., Staebler, R., Makar, P. A., Stroud, C. A., McLaren, R., Liu, P. S. K., O'Brien, J., Mittermeier, R. L., Zhang, J., Marson, G., Cober, S. G., Wolde, M., and Wentzell, J. J. B.: Differences between measured and reported volatile organic compound emissions from oil sands facilities in Alberta, Canada, Proc. Natl. Acad. Sci. U. S. A., 114, E3756-E3765, https://doi.org/10.1073/pnas.1617862114, 2017.

Liggio, J., Moussa, S. G., Wentzell, J., Darlington, A., Liu, P., Leithead, A., Hayden, K., O'Brien, J., Mittermeier, R. L., Staebler, R., Wolde, M., and Li, S. M.: Understanding the primary emissions and secondary formation of gaseous organic acids in the oil sands region of Alberta, Canada, Atmos. Chem. Phys., 17, 8411-8427, https://doi.org/10.5194/acp-17-8411-2017, 2017.

Makar, P. A., Akingunola, A., Aherne, J., Cole, A. S., Aklilu, Y. A., Zhang, J., Wong, I., Hayden, K., Li, S. M., Kirk, J., Scott, K., Moran, M. D., Robichaud, A., Cathcart, H., Baratzedah, P., Pabla, B., Cheung, P., Zheng, Q., and Jeffries, D. S.: Estimates of exceedances of critical loads for acidifying deposition in Alberta and Saskatchewan, Atmos. Chem. Phys., 18, 9897-9927, https://doi.org/10.5194/acp-18-9897-2018, 2018.

Marshall, T. L., Chaffin, C. T., Hammaker, R. M., and Fateley, W. G.: An introduction to open-path FT-IR atmospheric monitoring, Environ. Sci. Technol., 28, 5, 224-232, https://doi.org/10.1021/es00054a715, 1994.

Meyers, T. P., Hall, M. E., Lindberg, S. E., and Kim, K.: Use of the modified bowen-ratio technique to measure fluxes of trace gases, Atmos. Environ., 30, 3321-3329, https://doi.org/10.1016/1352-2310(96)00082-9, 1996.

Millet, D. B., Jacob, D. J., Custer, T. G., De Gouw, J. A., Goldstein, A. H., Karl, T., Singh, H. B., Sive, B. C., Talbot, R. W., Warneke, C., and Williams, J.: New constraints on terrestrial and oceanic sources of atmospheric methanol, Atmos. Chem. Phys., 8, 6887-6905, https://doi.org/10.5194/acp-8-6887-2008, 2008.

Monin, A. S., and Obukhov, A. M.: Basic laws of turbulent mixing in the surface layer of the atmosphere, Contrib. Geophys. Inst. Acad. Sci. USSR, 24, 25, 1954.

Oppenheimer, C., and Kyle, P. R.: Probing the magma plumbing of Erebus volcano, Antarctica, by open-path FTIR spectroscopy of gas emissions, J. Volcanol. Geotherm. Res., 177, 743-754, https://doi.org/10.1016/j.jvolgeores.2007.08.022, 2008.

Paton-Walsh, C., Smith, T. E. L., Young, E. L., Griffith, D. W. T., and Guérette, É. A.: New emission factors for Australian vegetation fires measured using open-path Fourier transform infrared spectroscopy - Part 1: Methods and Australian temperate forest fires, Atmos. Chem. Phys., 14, 11313-11333, https://doi.org/10.5194/acp-14-11313-2014, 2014.

Penner, T. J., and Foght, J. M.: Mature fine tailings from oil sands processing harbour diverse methanogenic communities, Can. J. Microbiol., 56, 459-470, https://doi.org/10.1139/W10-029, 2010.

Risacher, F. F., Morris, P. K., Arriaga, D., Goad, C., Nelson, T. C., Slater, G. F., and Warren, L. A.: The interplay of methane and ammonia as key oxygen consuming constituents in early stage development of Base Mine Lake, the first demonstration oil sands pit lake, Appl. Geochem., 93, 49-59, https://doi.org/10.1016/j.apgeochem.2018.03.013, 2018.

Rogers, T. M., Grimsrud, E. P., Herndon, S. C., Jayne, J. T., Kolb, C. E., Allwine, E., Westberg, H., Lamb, B. K., Zavala, M., Molina, L. T., Molina, M. J., and Knighton, W. B.: On-road measurements of volatile organic compounds in the Mexico City metropolitan area using proton transfer reaction mass spectrometry, Int. J. Mass Soectrom., 252, 26-37, https://doi.org/10.1016/j.ijms.2006.01.027, 2006.

Schäfer, K., Grant, R. H., Emeis, S., Raabe, A., von der Heide, C., and Schmid, H. P.: Areal-averaged trace gas emission rates from long-range open-path measurements in stable boundary layer conditions, Atmos. Meas. Tech., 5, 1571-1583, https://doi.org/10.5194/amt-5-1571-2012, 2012.

Schmid, H.P.: Source areas for scalars and scalar fluxes. Boundary-Layer Meteorol., **67,** 293–318, https://doi.org/10.1007/BF00713146, 1994.

Shephard, M. W., McLinden, C. A., Cady-Pereira, K. E., Luo, M., Moussa, S. G., Leithead, A., Liggio, J., Staebler, R. M., Akingunola, A., Makar, P., Lehr, P., Zhang, J., Henze, D. K., Millet, D. B., Bash, J. O., Zhu, L., Wells, K. C., Capps, S. L., Chaliyakunnel, S., Gordon, M., Hayden, K., Brook, J. R., Wolde, M., and Li, S. M.: Tropospheric Emission Spectrometer (TES) satellite observations of ammonia, methanol, formic acid, and carbon monoxide over the Canadian oil sands: Validation and model evaluation, Atmos. Meas. Tech., 8, 5189-5211, https://doi.org/10.5194/amt-8-5189-2015, 2015.

Shonkwiler, K. B., and Ham, J. M.: Ammonia emissions from a beef feedlot: Comparison of inverse modeling techniques using long-path and point measurements of fenceline NH_3, Agric. For. Meterol., 258, 29-42, https://doi.org/10.1016/j.agrformet.2017.10.031, 2018.

Siddique, T., Fedorak, P. M., MacKinnon, M. D., and Foght, J. M.: Metabolism of BTEX and Naphtha Compounds to Methane in Oil Sands Tailings, Environmental Science & Technology, 41, 2350-2356, 10.1021/es062852q, 2007.

Siddique, T., Penner, T., Semple, K., and Foght, J. M.: Anaerobic biodegradation of longer-chain n-alkanes coupled to methane production in oil sands tailings, Environ. Sci. Tech., 45, 5892-5899, https://doi.org/10.1021/es200649t, 2011.

Siddique, T., Penner, T., Klassen, J., Nesbø, C., and Foght, J. M.: Microbial communities involved in methane production from hydrocarbons in oil sands tailings, Environ. Sci. Tech., 46, 9802-9810, https://doi.org/10.1021/es302202c, 2012.

Simpson, I. J., Blake, N. J., Barletta, B., Diskin, G. S., Fuelberg, H. E., Gorham, K., Huey, L. G., Meinardi, S., Rowland, F. S., Vay, S. A., Weinheimer, A. J., Yang, M., and Blake, D. R.: Characterization of trace gases measured over Alberta oil sands mining operations: 76 speciated C_2–C_{10} volatile organic compounds (VOCs), CO_2, CH_4, CO, NO, NO_2, NO_y, O_3 and SO_2, Atmos. Chem. Phys., 10, 11931-11954, https://doi.org/10.5194/acp-10-11931-2010, 2010.

Simpson, I. J., Akagi, S. K., Barletta, B., Blake, N. J., Choi, Y., Diskin, G. S., Fried, A., Fuelberg, H. E., Meinardi, S., Rowland, F. S., Vay, S. A., Weinheimer, A. J., Wennberg, P. O., Wiebring, P., Wisthaler, A., Yang, M., Yokelson, R. J., and Blake, D. R.: Boreal forest fire emissions in fresh Canadian smoke plumes: C_1-C_{10} volatile organic compounds (VOCs), CO_2, CO, NO_2, NO, HCN and CH_3CN, Atmos. Chem. Phys., 11, https://doi.org/6445-6463, 10.5194/acp-11-6445-2011, 2011.

Small, C. C., Cho, S., Hashisho, Z., and Ulrich, A. C.: Emissions from oil sands tailings ponds: Review of tailings pond parameters and emission estimates, Journal of Petroleum Science and Engineering, 127, 490-501, https://doi.org/10.1016/j.petrol.2014.11.020, 2015.

Smith, T. E. L., Paton-Walsh, C., Meyer, C. P., Cook, G. D., Maier, S. W., Russell-Smith, J., Wooster, M. J., and Yates, C. P.: New emission factors for Australian vegetation fires measured using open-path Fourier Transform Infrared spectroscopy - Part 2: Australian tropical savanna fires, Atmos. Chem. Phys., 14, https://doi.org/11335-11352, 10.5194/acp-14-11335-2014, 2014.

Thoma, E. D., Green, R. B., Hater, G. R., Goldsmith, C. D., Swan, N. D., Chase, M. J., and Hashmonay, R. A.: Development of EPA OTM 10 for landfill applications, J. Environ. Eng., 136, 769-776, https://doi.org/10.1061/(ASCE)EE.1943-7870.0000157, 2010.

Whaley, C. H., Makar, P. A., Shephard, M. W., Zhang, L., Zhang, J., Zheng, Q., Akingunola, A., Wentworth, G. R., Murphy, J. G., Kharol, S. K., and Cady-Pereira, K. E.: Contributions of natural and anthropogenic sources to ambient ammonia in the Athabasca Oil Sands and north-western Canada, Atmos. Chem. Phys., 18, 2011-2034, https://doi.org/10.5194/acp-18-2011-2018, 2018.

Wiacek, A., Li, L., Tobin, K., and Mitchell, M.: Characterization of trace gas emissions at an intermediate port, Atmos. Chem. Phys., 18, 13787-13812, https://doi.org/10.5194/acp-18-13787-2018, 2018.

Wu, R. T., Chang, S.-Y., Chung, Y. W., Tzou, H. C., and Tso, T.-L.: FTIR remote sensor measurements of air pollutants in the petrochemical industrial park, Proc. SPIE 2552, Infrared Technology XXI, 1995, 719-727, https://doi.org/10.1117/12.218271, 1995.

Yeh, S., Jordaan, S. M., Brandt, A. R., Turetsky, M. R., Spatari, S., and Keith, D. W.: Land use greenhouse gas emissions from conventional oil production and oil sands, Environ. Sci. Tech., 44, 8766-8772, https://doi.org/10.1021/es1013278, 2010.

Yokelson, R. J., Griffith, D. W. T., and Ward, D. E.: Open-path Fourier Transform Infrared studies of large-scale laboratory biomass fires, J. Geophys. Res. Atmos., 101, 21067-21080, https://doi.org/10.1029/96JD01800, 1996.

Yokelson, R. J., Susott, R., Ward, D. E., Reardon, J., and Griffith, D. W. T.: Emissions from smoldering combustion of biomass measured by open-path Fourier Transform Infrared spectroscopy, J. Geophys. Res. Atmos., 102, 18865-18877, https://doi.org/10.1029/97JD00852, 1997.

Yokelson, R. J.: Emissions of formaldehyde, acetic acid, methanol, and other trace gases from biomass fires in North Carolina measured by airborne Fourier Transform Infrared spectroscopy, J. Geophys. Res. Atmos., 104, 30109-30125, https://doi.org/10.1029/1999JD900817, 1999.

Yokelson, R. J., Karl, T., Artaxo, P., Blake, D. R., Christian, T. J., Griffith, D. W. T., Guenther, A., and Hao, W. M.: The tropical forest and fire emissions experiment: Overview and airborne fire emission factor measurements, Atmos. Chem. Phys., 7, 5175-5196, https://doi.org/10.5194/acp-7-5175-2007, 2007.

Yokelson, R. J., Burling, I. R., Gilman, J. B., Warneke, C., Stockwell, C. E., De Gouw, J., Akagi, S. K., Urbanski, S. P., Veres, P., Roberts, J. M., Kuster, W. C., Reardon, J., Griffith, D. W. T., Johnson, T. J., Hosseini, S., Miller, J. W., Cocker Iii, D. R., Jung, H., and Weise, D. R.: Coupling field and laboratory measurements to estimate the

emission factors of identified and unidentified trace gases for prescribed fires, Atmos. Chem. Phys., 13, 89-116, https://doi.org/10.5194/acp-13-89-2013, 2013.

You, Y., Staebler, R. M., Moussa, S. G., Su, Y., Munoz, T., Stroud, C., Zhang, J., and Moran, M. D.: Long-path measurements of pollutants and micrometeorology over Highway 401 in Toronto, Atmos. Chem. Phys., 17, 14119-14143, https://doi.org/10.5194/acp-17-14119-2017, 2017.

You, Y., Staebler, R. M.: Moussa, S. G., Beck, J., Mittermeier, R. L.: Methane emissions from an oil sands tailings pond: A quantitative comparison of fluxes derived by different methods, Atmos. Meas. Tech. Discuss., https://doi.org/10.5194/amt-2020-116, in review, 2020.

Zhang, L., Cho, S., Hashisho, Z., and Brown, C.: Quantification of fugitive emissions from an oil sands tailings pond by eddy covariance, Fuel, 237, 457-464, https://doi.org/10.1016/j.fuel.2018.09.104, 2019.

Tables

Table 1 Spectral windows of OP- FTIR spectra for retrieving mole fractions of pollutants in this study.

Pollutant name	Chemical formula	Spectral Window (cm^{-1})	Interference gases	Threshold correlation coefficient[a]	Detection limit[c]	Paths
Methane	CH_4	3006-3021	H_2O	0.95	1.1 ppb	All three
Ammonia	NH_3	957-973	H_2O, CO_2	0.3	1.1 ppb	All three
Methanol	CH_3OH	1020-1040	H_2O, NH_3, O_3, C_2H_5OH, C_6H_6	0.3	1.1 ppb	All three
Butane[b]	n-C_4H_{10}	2804-3001	H_2O, CH_4, CH_3OH, HCHO, n-C_7H_{16}, n-C_6H_{14}, n-C_8H_{18}, $CH_3CH(CH_3)C_3H_7$	0.1	1.1 ppb	All three
Octane[b]	n-C_8H_{18}	2804-3001	H_2O, CH_4, CH_3OH, HCHO, n-C_7H_{16}, n-C_6H_{14}, $CH_3CH(CH_3)C_3H_7$, $C_2H_5CH(CH_3)C_2H_5$	0.1	0.9 ppb	All three
Formaldehyde	HCHO	2730-2800	H_2O, CO_2, CH_4	0.2	2.3 ppb	Bottom only
Carbon dioxide	CO_2	2030-2133	H_2O, CO	0.8	-	Bottom only

[a] Threshold correlation coefficient is a input for OPUS_RS when performing fitting analysis of FTIR spectra. When the correlation coefficient between measured spectrum and reference spectrum with the defined spectral window is below this threshold, that pollutant is not "identified" and the mole fraction is reported as zero in OPUS_RS (You et al., 2017).

[b] Butane and octane mixing ratio are quantified as two surrogates to quantify a "total alkane" mixing ratio = Butane + Octane (Thoma et al., 2010).

[c] Detection limit is calculated by converting 3σ of the noise of the measurements with a retroreflector distance of 225m by Bruker to 3σ of the noise with 200m in this study.

Table 2 Summary of fluxes from OP-FTIR measurements. Results are area weight-averaged fluxes from the pond.

All fluxes in g $m^{-2}d^{-1}$	Flux method	Q_25%	Median	Q_75%	Mean[a]
CH_4	Tower EC	5.6	7.4	9.8	7.8±1.1
	FTIR gradient	2.3	3.8	6.0	4.3 ± 0.9
	IDM	3.6	5.2	6.6	5.4± 0.4
NH_3	gradient	0.03	0.04	0.09	0.05 ± 0.01
	IDM	0.06	0.09	0.15	0.11 ± 0.01
Total alkane	gradient	0.25	0.70	1.60	1.05 ± 0.28
	IDM	0.57	0.94	1.56	1.33 ± 0.10

[a] Errors with the mean fluxes are calculated with a "top-down" approach: the average of standard deviations of fluxes from five periods when the fluxes displayed high stationarity.

Deleted: 4.2
Deleted: 5.9
Deleted: 7.9
Deleted: 6.1
Deleted: 0.5
Deleted: 1.8
Deleted: 3.0
Deleted: 4.8
Deleted: 3.4
Deleted: 0.7
Deleted: 0.02
Deleted: 0.03
Deleted: 0.07
Deleted: 0.04
Deleted: ± 0.01
Deleted: 0.20
Deleted: 0.56
Deleted: 1.28
Deleted: 0.84
Deleted: 0.22-

Figures

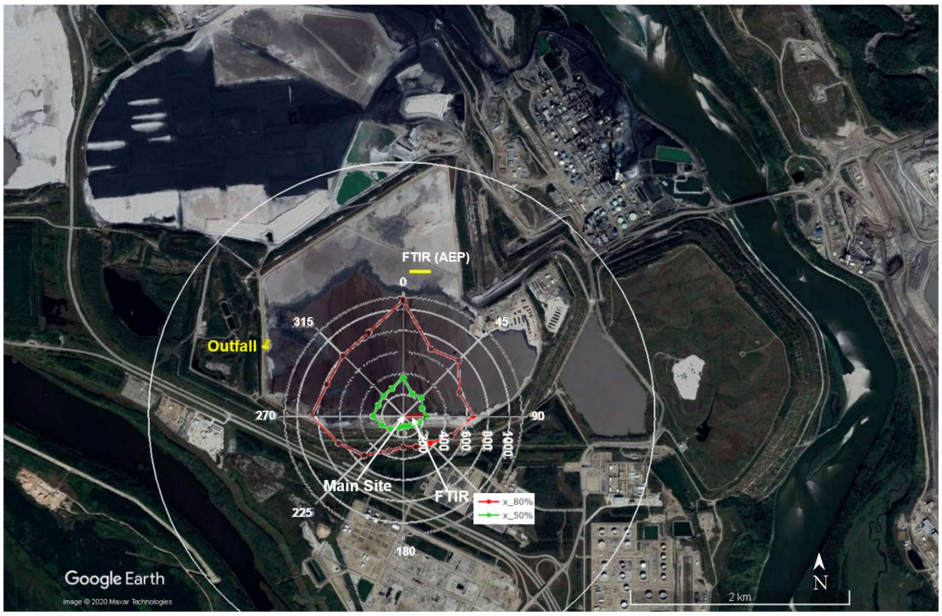

Figure 1 Map of the site: open-path FTIR on the south shore marked in red, open-path FTIR of AEP on the north shore marked in yellow, and the outfall on the west side. The colored rose plot shows 50% and 80% contribution distances for eddy covariance fluxes at 18m using the Flux Footprint Prediction (FFP) model (Kljun et al. (2015)). The unit of contribution distances is in meters. The white circle labels the 2.3 km distance from the main site, equivalent to 100 times the height of the highest point of the top FTIR path. This figure is adapted from You et al., (2020) Figure 1.

Formatted: English (Canada)

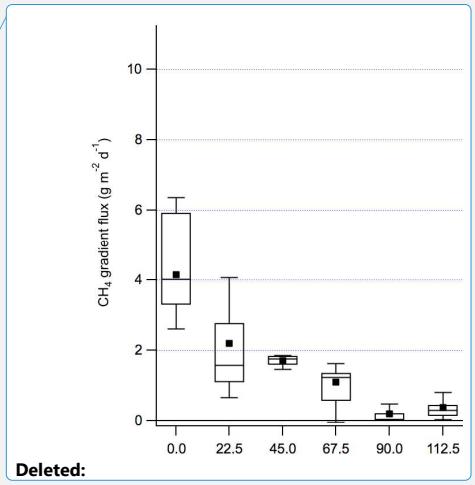

Deleted:

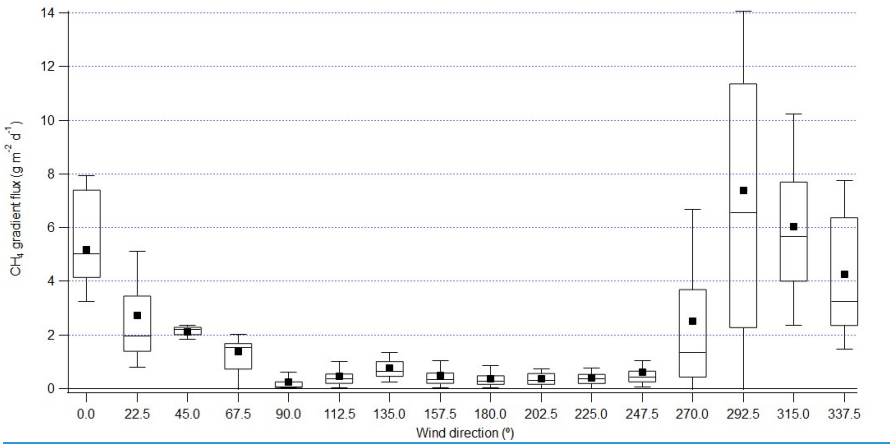

Figure 2 Gradient flux of CH_4 from FTIR binned by wind direction in 22.5-degree bins. Lower and upper bounds of the box plot are 25th and 75th percentile; the line in the box marks the median and the black square labels the mean; the whiskers label the 10th and 90th percentile.

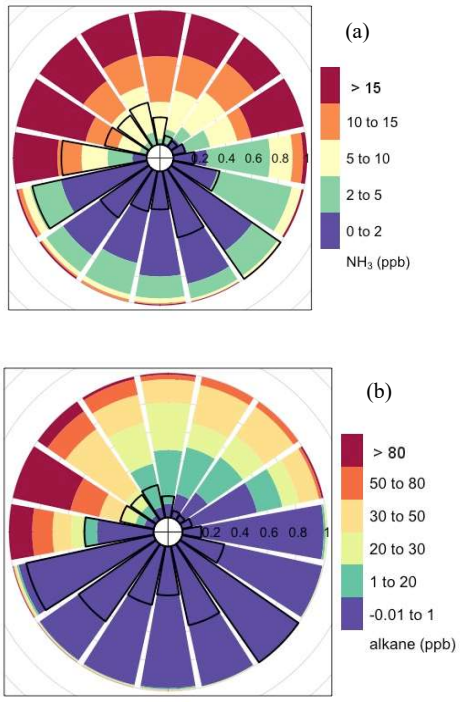

Figure 3Normalised rose plot of NH_3 (a) and total alkane (b) mole fractions from FTIR bottom path. Colors represent mole fraction in ppb. The length of each colored segment presents the time fractions of that mole fraction range in each direction bin. The radius of the black open sectors indicates the frequency of wind in each direction bin; angle represents wind direction, straight up is north, and straight left is west.

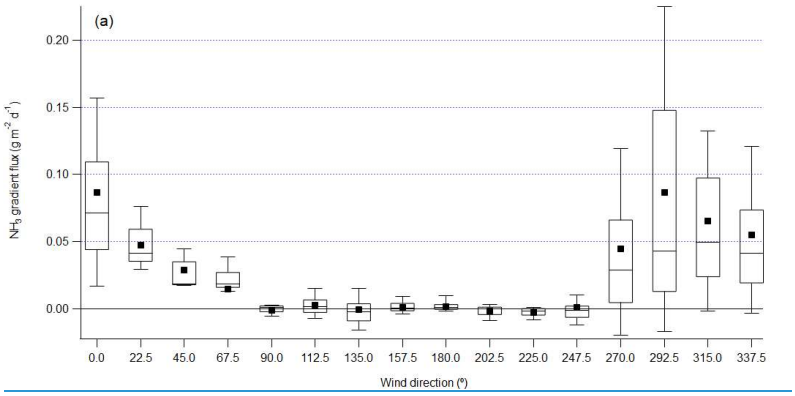

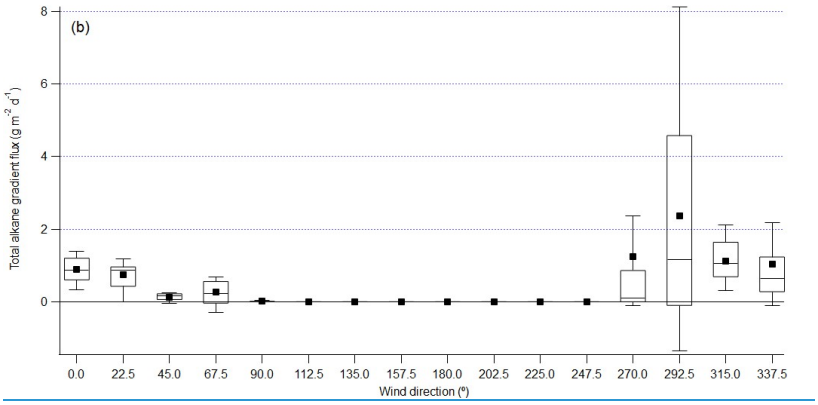

Figure 4 Gradient flux of NH_3 (a) and total alkane (b) from FTIR top-bottom path binned by wind direction in 22.5-degree bins. Lower and upper bounds of the box plot are 25th and 75th percentile; the line in the box marks the median and the black square labels the mean; the whiskers label the 10th and 90th percentile.

Deleted:

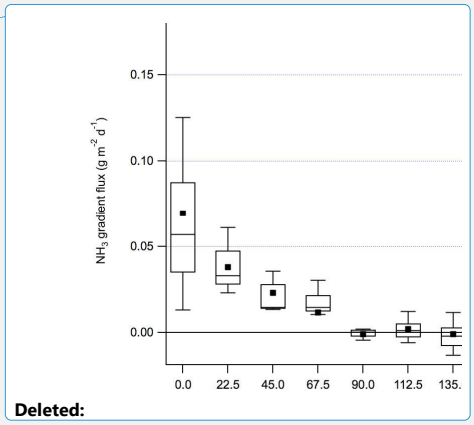

Deleted: *<object>*

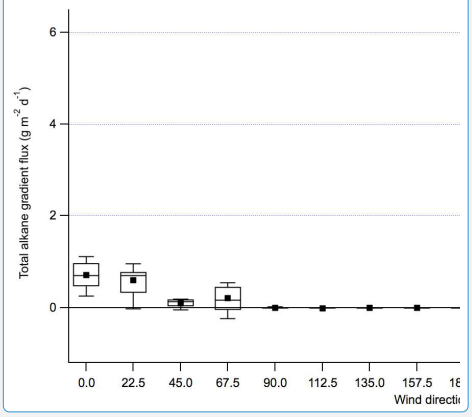

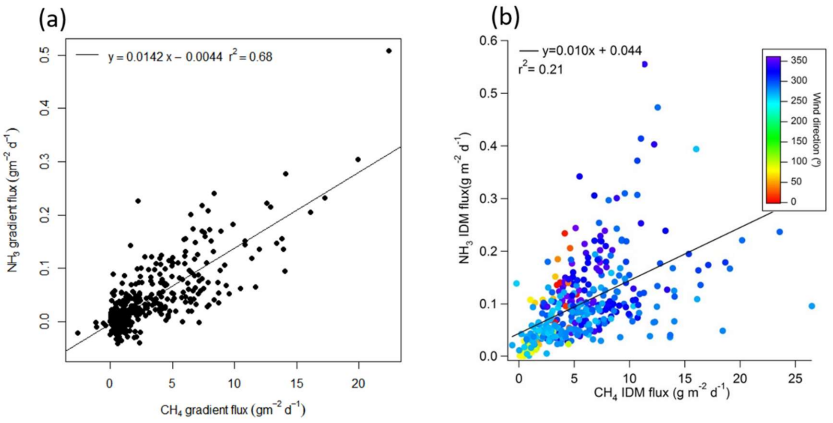

Figure 5 (a): NH_3 gradient flux compared to CH_4 gradient flux; (b): NH_3 IDM flux compared to CH_4 IDM flux

790

Deleted:

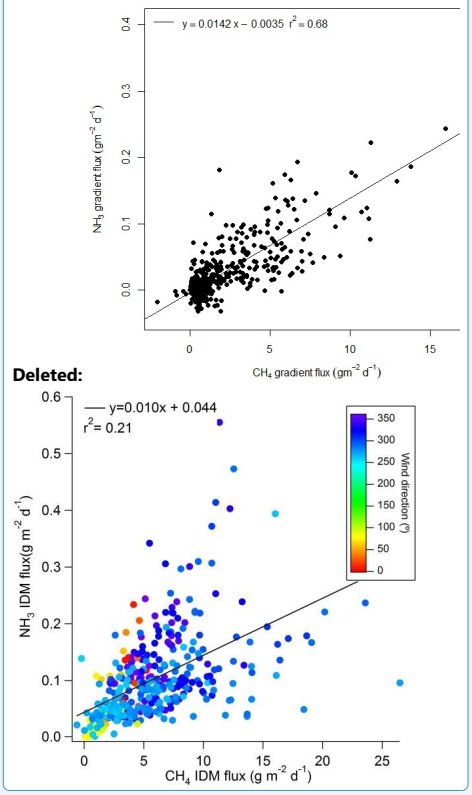

Supplemental material: Gas emissions from an oil sands tailings pond with open-path FTIR measurements

Yuan You[1,§], Samar G. Moussa[1], Lucas Zhang[2], Long Fu[2], James Beck[3], Ralf M. Staebler[1]

[1] Air Quality Research Division, Environment and Climate Change Canada (ECCC), Toronto, M3H 5T4, Canada
[2]Alberta Environment and Parks, Edmonton, T5J, 5C6, Canada
[3]Suncor Energy Inc., Calgary, T2P 3Y7, Canada
[§]Now at Department of Physics, University of Toronto, Toronto, M5S 1A7, Canada

Correspondence to: Ralf M. Staebler (ralf.staebler@canada.ca)

1. Methane mole fractions, vertical profiles, and gradient fluxes

Calibration of retrieved CH_4 mole fraction from OP-FTIR

The amplitude of spectra for all the three paths varied substantially over the study period, especially for the top path. As a proxy for the spectral amplitude, the signal-to-noise ratio (SNR) of the CH_4 fitting was used. The CH_4, NH_3, CH_3OH and HCHO mole fraction for all three paths when this SNR dropped fast, or stayed below 10 were flagged. 3% and 13% of the measurements from bottom and top path were flagged and invalidated from further mole fraction gradient and flux calculations.

Since CH_4 mole fraction was also continuously measured by cavity ring-down spectroscopy (CRDS) at four heights during the study, the measurements at 4m were compared to CH_4 mole fraction retrieved from the FTIR bottom path to calibrate the retrieved CH_4 mole fraction from three paths of this OP-FTIR system.

Each CRDS in this study was calibrated before and after the campaign, and CH_4 mole fraction from three CRDS at the same height was well compared (r^2>0.96, slope=0.98- 1.01, intercept=0.01-0.02 ppm). Therefore, CH_4 mole fraction retrieved from FTIR all three paths were calibrated by the linear relationship in Fig. S2:

$$[CH_4]\_FTIR\_calibrated=1.2015\times[CH_4]\_FTIR\_retrieved - 0.397 \quad \text{(S. 1)}$$

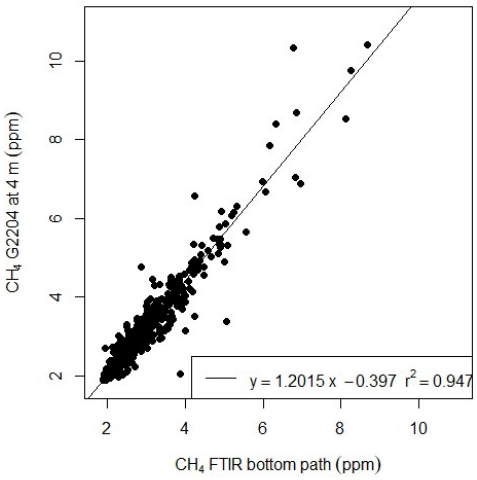

820 **Figure S 1 CH_4 mole fraction retrieved from FTIR bottom path compared to CH_4 mole fraction measured by CRDS (G2204) at 4m. Data are half-hour averaged results.**

Mole fractions and vertical profiles with gradient fluxes

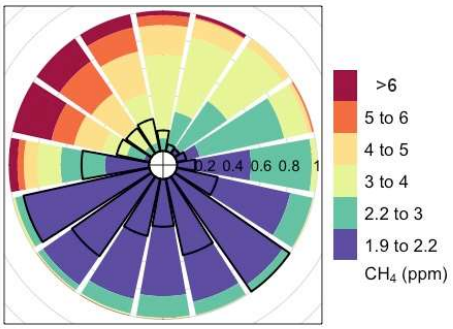

Figure S 2 Normalised rose plot of CH_4 mole fractions from FTIR bottom path. Colors represent CH_4 mole fractions. The length of each colored segment presents the time fractions of that mixing ratio in each direction bin. The radius of the black open sectors indicates the frequency of wind in each direction bin; angle represents wind direction: straight up is north and straight left is west.

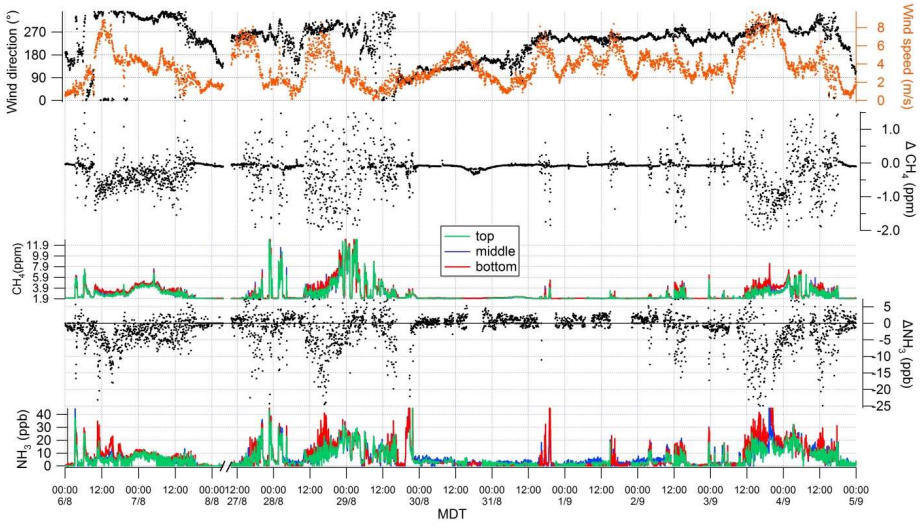

Figure S 3 Time series of wind direction, wind speed, difference in CH_4 mole fractions from the top and bottom paths, CH_4 mole fractions, difference in NH_3 mole fractions from the top and bottom paths, and NH_3 mole fractions, from Aug 6th to 8th, and from Aug 27th to Sept 5th. MDT = Mountain Daylight savings Time.

In the analysis of methane vertical profile below, all the mole fractions measurements (half-hour averages) were taken from the Picarro G2204 at 4, 8, 18, and 32m. There are 271 half-hours in total when the wind was from the pond. About 83% of the half-hour periods when the wind was from the pond direction, the CH_4 vertical profiles are similar to Fig. S4. Within this 83% of periods, some profiles are close to linear, and others are not strict decreasing trend with height. For the rest of 17% of half-hour periods, the CH_4 vertical profiles are closer to logarithmic (Fig. S6). Therefore, CH_4 vertical profiles are considered linear over the entire period for calculating gradient flux with OP-FTIR measurement.

In addition, those half-hour periods when logarithmic relationship is better than linear to describe the vertical profile are mainly (65%) associated with wind speed greater than 6m/s (Fig. S7). For the majority of the time (85%) when the wind was from the pond, wind speed was less than 6m/s (Fig. S7).

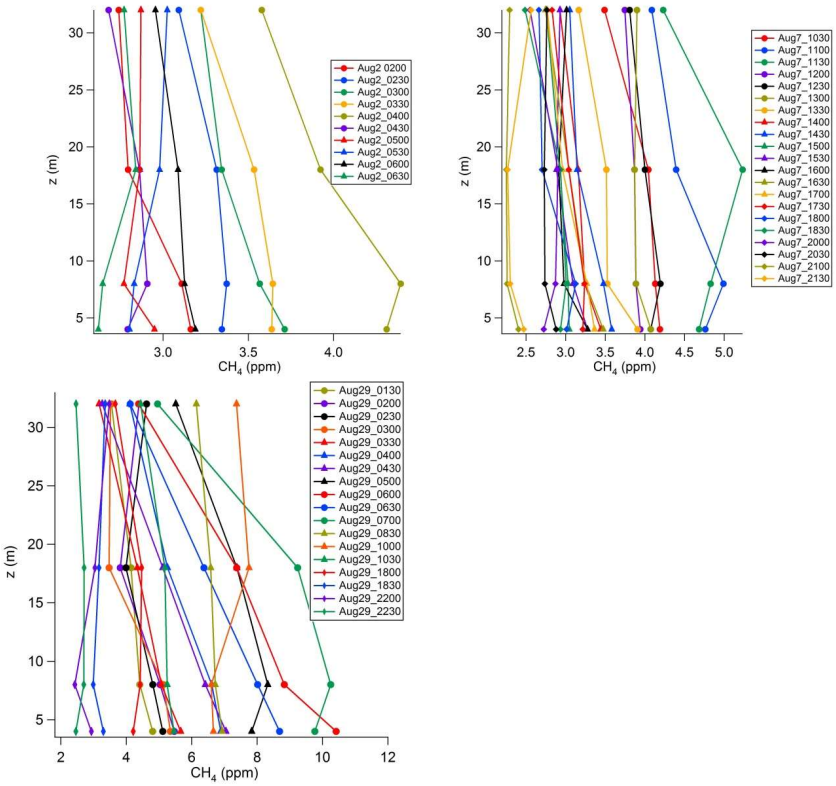

Figure S 4 Examples of observed CH_4 mole fractions vertical profile, when the profiles are close to linear.

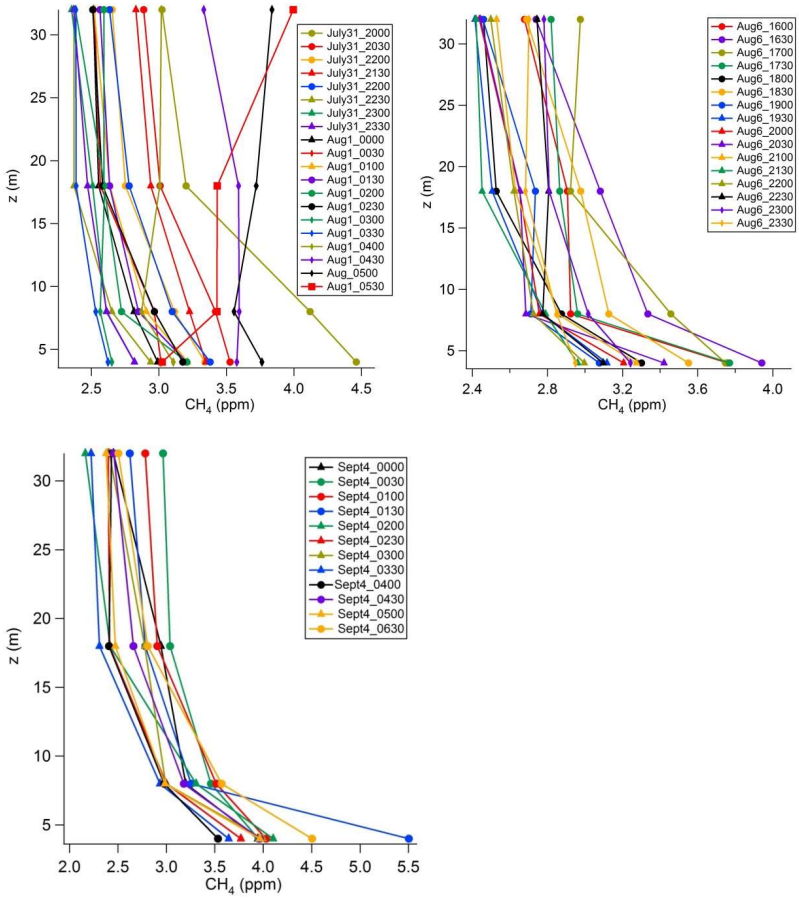

Figure S 5 Examples of observed CH_4 mole fractions vertical profile, when the profiles are close to logarithmic.

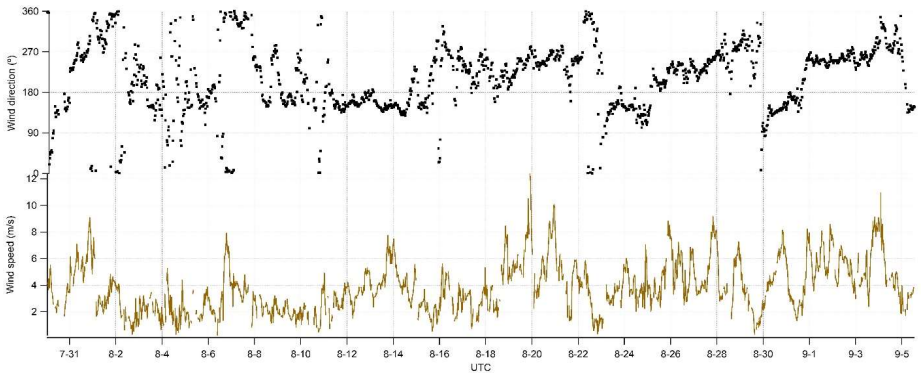

Figure S 6 Time series of wind direction and wind speed measured at 18m over the entire project.

To compare to the assumption of linear vertical profile of CH_4 mole fractions, the calculation of K_c for the assumption of logarithmic vertical profile is also listed here. The representative average height of the FTIR top path with a logarithmic vertical profile would be $Z_{top} = \sqrt{23 \times 1} = 4.8\ m$. Then, K_c for gradient flux calculated from the top-to-bottom path gradient is adjusted logarithmically based on the $K_{c\_2,4}$ calculated from point measurements at 8m and 32m on the tower:

$$F_{gradient_{FTIR}} = -K_{c\_FTIR\_log} \times \frac{\partial c}{\partial z} = \frac{-K_{c_{FTIR\_log}} * \partial c}{z * \ln(\frac{z_2}{z_1})} = -\frac{K_{mFTIR\_log}}{K_{m8,32m}} \times K_{c_{8,32m}} \times \frac{\partial c}{\sqrt{4.79 \times 1} \times \ln(\frac{4.79}{1})} = -0.291 \times \frac{K_{mFTIR\_log}}{K_{m8,32m}} \times K_{c_{8,32m}} \times \partial c \text{ (S. 2)},$$

where z is the height for which flux is calculated (Thompson and Pinker, 1981).

$\frac{K_{mFTIR\_log}}{K_{m8,32m}}$ is a function of stability (z/L) and is calculated with eq.(5) and (6) in the main text. The gradient flux of CH_4 with logarithmic vertical profile is calculated with eq. (S2) and the area-weighted average flux from the pond sectors is 4.1 $gm^{-2}d^{-1}$,which is 19% greater than the gradient flux calculated with linear vertical profile.

Beside top-bottom paths of CH_4 mole fractions gradient, middle-bottom paths of gradient can also be used to calculate CH_4 gradient fluxes. The results are summarised in the first row of Table S1 to compare to gradient fluxes with top-bottom paths CH_4 gradients. The area-weighted averaged fluxes with middle-bottom paths is 29% lower than the area-weighted averaged fluxes with top-bottom paths (Table S1).

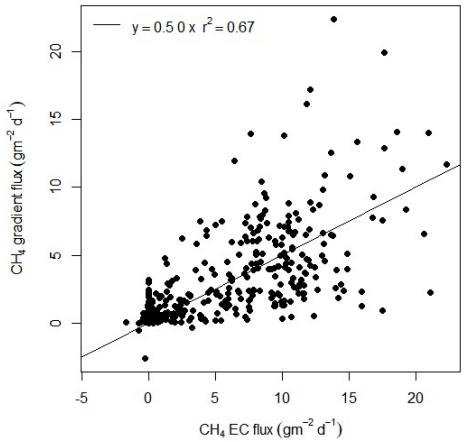

Figure S 7 CH_4 gradient flux from FTIR compared with EC flux.

880

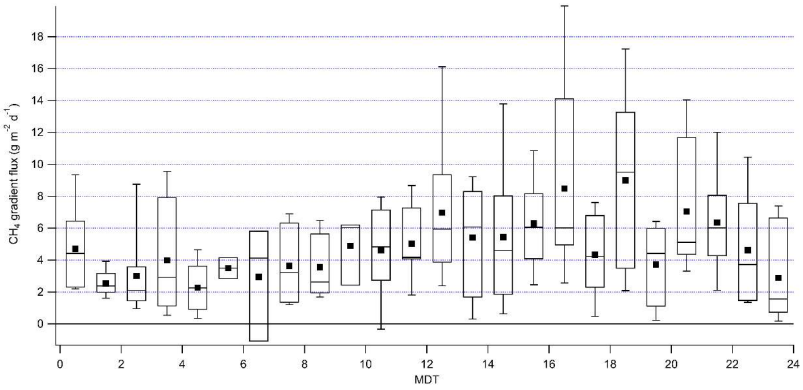

885 **Figure S 8 Diurnal variation of CH_4 gradient flux from FTIR, when the wind came from the pond direction. MDT = Mountain Daylight savings Time. Lower and upper bounds of the box plot are 25th and 75th percentile; the line in the box marks the median and the black square labels the mean; the whiskers label the 10th and 90th percentile.**

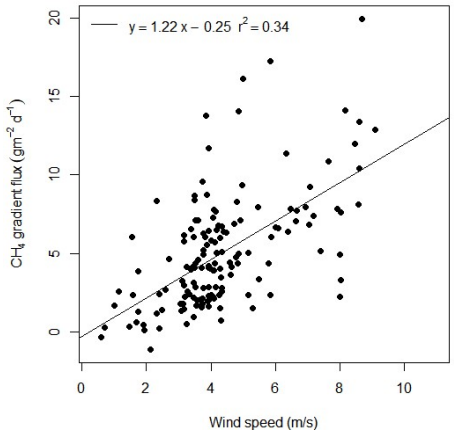

890

Figure S 9 CH_4 gradient flux when the wind was from the pond.

IDM flux of CH4 with two approaches of determining background mole fraction input

IDM fluxes of CH_4 with input from FTIR. Fluxes comparison with background mole fraction using ECCC measurement at south, and AEP measurements at north:

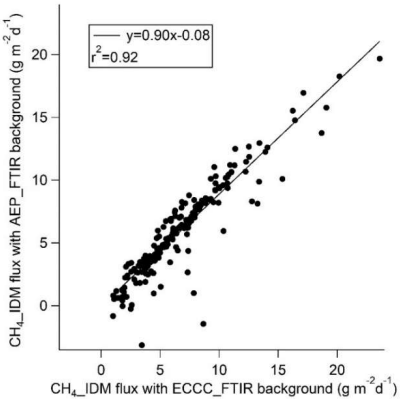

Figure S 10 comparison of CH_4 IDM fluxes with input background mole fraction from the south and north measurements.

The half-hour IDM fluxes with these two approaches agree well (slope = 0.9, r^2=0.92). The sector-area-weight-averaged IDM fluxes with two approaches are also within 20% difference. The interquartile ranges overlap (Table S1).

2. NH_3

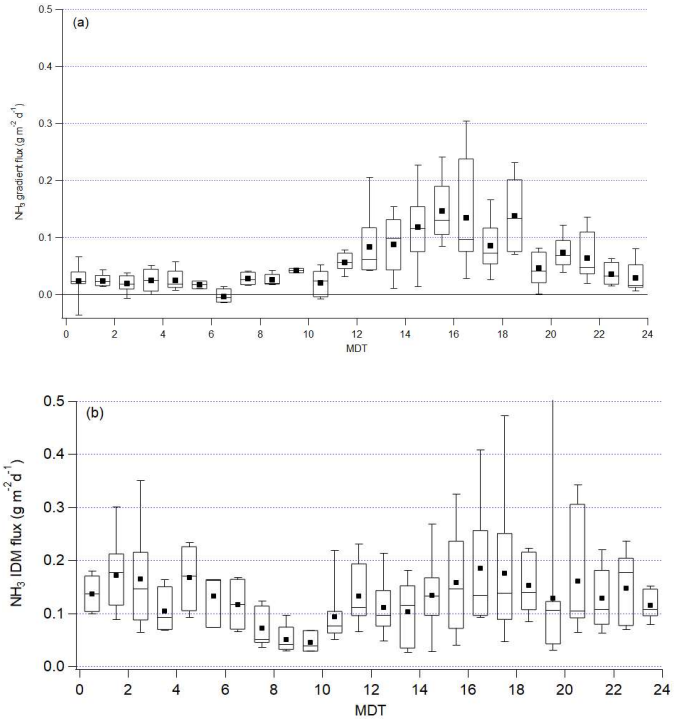

Figure S 11 Diurnal variations of NH_3 gradient flux derived from top-bottom paths (a) and IDM flux (b) when the wind was from the pond direction. MDT = Mountain Daylight savings Time. Lower and upper bounds of the box plot are 25th and 75th percentile; the line in the box marks the median and the black square labels the mean; the whiskers label the 10th and 90th percentile.

915

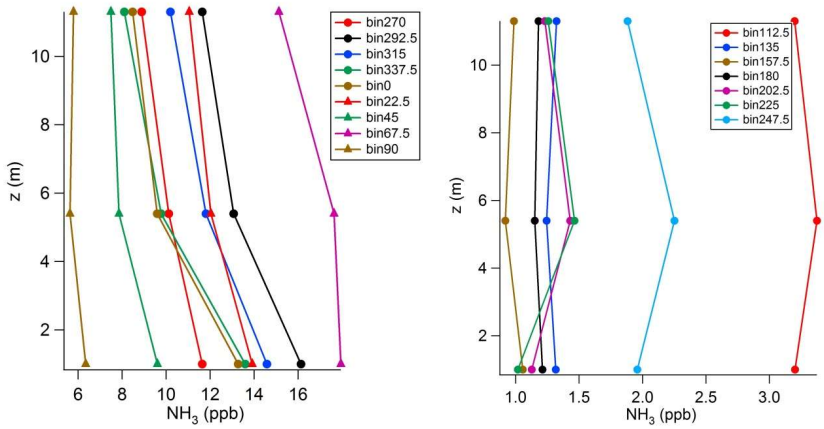

Figure S 12 NH_3 mole fraction vertical profile after averaging in 16 wind direction sectors. The height z for the three paths are the height of the middle point of each path.

3. Total alkane

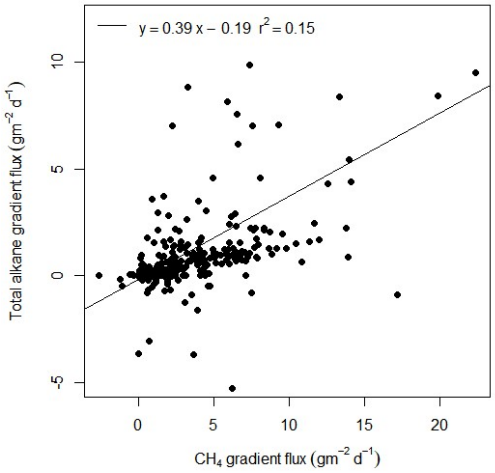

Figure S 13 Total alkane gradient flux compared to CH_4 gradient flux, both derived from OP-FTIR top and bottom paths.

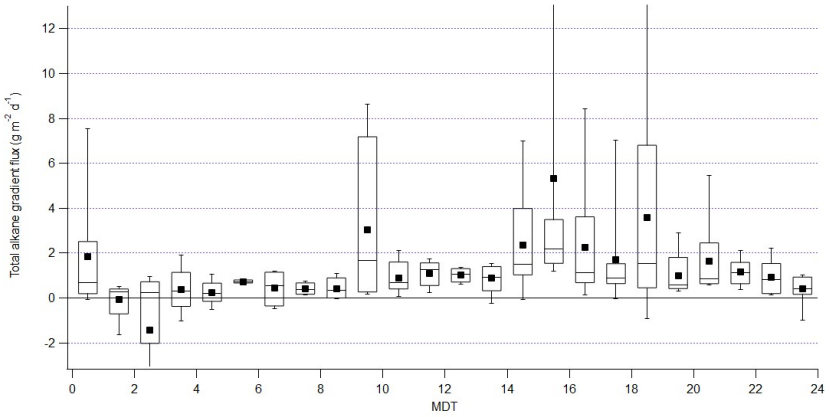

Figure S 14 Diurnal variation of total alkane gradient flux when the wind was from the pond direction. MDT = Mountain Daylight savings Time. Lower and upper bounds of the box plot are 25th and 75th percentile; the line in the box marks the median and the black square labels the mean; the whiskers label the 10th and 90th percentile.

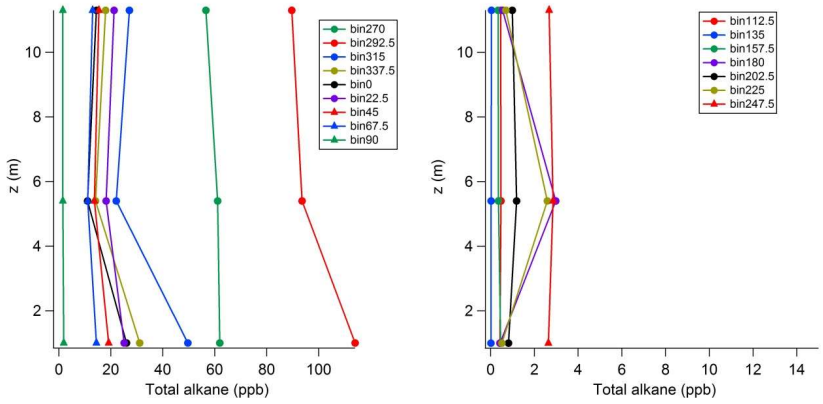

Figure S 15 Total alkane mole fraction vertical profile after averaging in 16 wind direction sectors. The height z for the three paths are the height of the middle point of each path.

4. Methanol (CH_3OH)

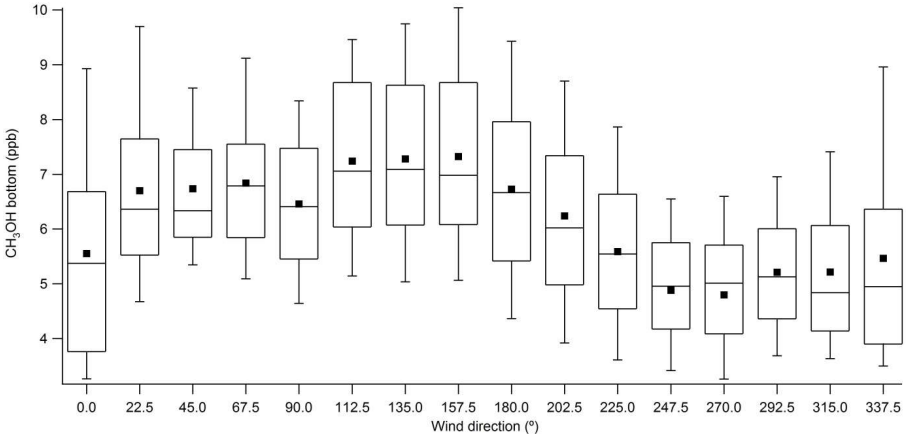

Figure S 16 CH_3OH mole fraction retrieved from the FTIR bottom path, binned in 22.5° sectors. Lower and upper bounds of the box plot are 25th and 75th percentile; the line in the box marks the median and the black square labels the mean; the whiskers label the 10th and 90th percentile.

5. Flux results with the slant path approach from Flesch et al. (2016)

As briefly discussed in the introduction of the main text, Flesch et al., (2016) deployed OP-FTIR measurement with "slant path" configuration, and derived emission rates of N_2O and NH_3 by flux-gradient method. To compare the methods we used to calculate gradient fluxes with their approach, we also performed similar calculation. The derived u_* and L directly from sonic anemometer measurement at 8m on the tower, mole fraction difference between top and bottom path of FTIR, and calculated S_c were plugged in equation (9) in Flesch et al., (2016). In this study, calculated S_c is allowed to vary with dynamic stability (You et al. (2020) Fig. 3), while in Flesch et al. (2016) S_c was a constant 0.64. The time series of half-hour gradient fluxes of CH_4, NH_3 and total alkane were calculated. Area weight-averaged fluxes were calculated and summarized in Table S1. Compared to gradient flux results with our approach modified Bowen ratio, CH_4, NH_3 and total alkane fluxes with the "slant path" flux-gradient method are 24%, 25%, and 30% smaller.

Tables

Table S1 Summary of CH_4 IDM fluxes with two background approaches, and gradient fluxes with approach from Flesch et al. (2016).

($g\ m^{-2}\ d^{-1}$)	Q_25%	median	Q_75%	mean[a]
CH_4_gradient flux with middle-bottom paths	1.5	2.6	4.1	3.0 ± 1.3
CH_4_IDM flux_with ECCC background	3.6	5.2	6.6	5.4 ± 0.4
CH_4_IDM flux_with AEP background	2.9	4.4	5.6	4.3 ± 0.6
CH_4 gradient flux with approach from Flesch et al. (2016)	1.5	2.9	4.6	3.3 ± 1.3
NH_3 gradient flux with approach from Flesch et al. (2016)	0.01	0.03	0.06	0.04 ± 0.01
Total alkane gradient flux with approach from Flesch et al. (2016)	0.16	0.50	1.08	0.74 ± 0.15

[a] Errors with the mean fluxes are calculated with an integrative approach: the average of observed standard deviations of fluxes from five periods when the fluxes displayed high stationarity.

Reference

Kljun, N., Calanca, P., Rotach, M. W., and Schmid, H. P.: A simple two-dimensional parameterisation for Flux Footprint Prediction (FFP), Geosci. Model Dev., 8, 3695-3713, http://doi.org/10.5194/gmd-8-3695-2015, 2015.

Thompson, O. E., and Pinker, R. T.: An error analysis of the Thornthwaite-Holzman equations for estimating sensible and latent heat fluxes over crop and forest canopies, J. Appl. Meteorol., 20, 250-254, 1981.